Journal Pre-proofs

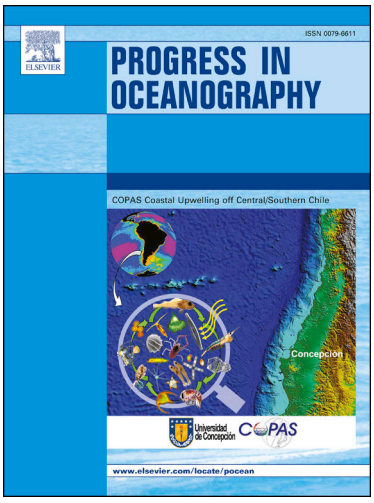

Dissolved and suspended organic matter dynamics in the Cape Verde Frontal Zone (NW Africa)

S. Valiente, B. Fernández-Castro, R. Campanero, A. Marrero-Díaz, A. Rodríguez-Santana, M.D. Gelado-Cabellero, M. Nieto-Cid, A. Delgado-Huertas, J. Arístegui, X.A. Álvarez-Salgado

PII: S0079-6611(21)00210-X
DOI: https://doi.org/10.1016/j.pocean.2021.102727
Reference: PROOCE 102727

To appear in: *Progress in Oceanography*

Received Date: 20 April 2021
Revised Date: 21 August 2021
Accepted Date: 3 December 2021

Please cite this article as: Valiente, S., Fernández-Castro, B., Campanero, R., Marrero-Díaz, A., Rodríguez-Santana, A., Gelado-Cabellero, M.D., Nieto-Cid, M., Delgado-Huertas, A., Arístegui, J., Álvarez-Salgado, X.A., Dissolved and suspended organic matter dynamics in the Cape Verde Frontal Zone (NW Africa), *Progress in Oceanography* (2021), doi: https://doi.org/10.1016/j.pocean.2021.102727

Dissolved and suspended organic matter dynamics in the Cape Verde Frontal Zone (NW Africa)

S. Valiente[a,b], B. Fernández-Castro [b,c], R. Campanero[a,b], A. Marrero-Díaz[d], A. Rodríguez-Santana[d], M.D. Gelado-Cabellero[e], M. Nieto-Cid[b,f], A. Delgado-Huertas[a], J. Arísteguig, X.A. Álvarez-Salgado[b]

[a] CSIC Instituto Andaluz de Ciencias de la Tierra (IACT–CSIC), Granada, Spain

[b] CSIC Instituto de Investigacións Mariñas (IIM–CSIC), Vigo, Spain

[c] Ocean and Earth Science, National Oceanography Center Southampton, University of Southampton, Southampton, UK

[d] Departamento de Física, Universidad de Las Palmas de Gran Canaria, Las Palmas de Gran Canaria, Spain

[e] Departamento de Química, Universidad de Las Palmas de Gran Canarias, Las Palmas, Spain

[f] Instituto Español de Oceanografía (IEO), Centro Oceanográfico de A Coruña, A Coruña, Spain

[g] Instituto de Oceanografía y Cambio Global, Universidad de Las Palmas de Gran Canaria, Telde, Spain

- CVFZ and Cape Blanc filament interaction dictates meso-scale DOM and POM distributions
- DOM and suspended POM have a minor contribution to the oxygen demand of the CVFZ
- Mesopelagic respiration in the CVFZ is primarily supported by sinking POM
- Transport and biogeochemical processes in the CVFZ reshape water masses properties

Abstract

The Cape Verde Frontal Zone (CVFZ) is a highly dynamic region located in the southern boundary of the Canary Current Eastern Boundary Upwelling Ecosystem. Due to the interaction of the Cape Verde Front with the Mauritanian coastal upwelling, the area features large vertical and horizontal export fluxes of organic matter. While the flux, composition and biogeochemical role of sinking organic matter have been thoroughly studied, much less attention has been paid to the dissolved (DOM) and suspended particulate (POM) organic matter fractions. Full-depth profiles of DOM and POM were recorded during an oceanographic cruise in the CVFZ, with four consecutive transects defining a box embracing the giant filament of Cape Blanc and the Cape Verde front. The distributions of DOM and POM and their C:N stoichiometric ratios in the epipelagic layer

were strongly influenced by the position of the transects relative to the giant filament and the front. Geographical heterogeneity in POM and DOM distributions and elemental composition was also observed within each of the different water masses of contrasting origin present in the area (North and South Atlantic Central Water, Subpolar Mode Water, Mediterranean Water, Antarctic Intermediate Water, Labrador Sea Water and North East Atlantic Deep Water). These facts suggest that water masses properties are re-shaped by biogeochemical processes occurring within the CVFZ. Nevertheless, our analysis indicates that DOM and POM mineralisation represents only 8.1% of the inorganic carbon and 17.8% of the inorganic nitrogen produced by the local mineralisation of organic matter. Intense lateral export of POM and DOM out of the boundaries of the CVFZ is the likely reason behind these low contributions, which confirm the prominent role of sinking fluxes of organic matter for mineralisation processes in this region. The DOM distribution in the CVFZ interior is apparently affected by the dissolution of fast sinking particles.

Keywords: Dissolved organic matter; particulate organic matter; water masses; carbon cycling; nitrogen cycling; Cape Verde Frontal Zone

List of acronyms

AA	Modified Antarctic Intermediate Water
AOU	Apparent oxygen utilization
Chl-a	Chlorophyll a
CVF	Cape Verde Front (when referring exclusively to the Front)
CVFZ	Cape Verde Frontal Zone (when referring to the entire study area)
DCM	Deep chlorophyll maximum
DOC	Dissolved organic carbon
DOM	Dissolved organic matter
DON	Dissolved organic nitrogen
EBUE	Eastern Boundary Upwelling Ecosystem
ENACW	Eastern North Atlantic Central Water
ENACW_15	Eastern North Atlantic Central Water of 15 ºC
ENACW_12	Eastern North Atlantic Central Water of 12 ºC
LNEADW	Lower North East Atlantic Deep Water
LSW	Labrador Sea Water
MMW	Madeira Mode Water
MW	Mediterranean Water
NEADW	North East Atlantic Deep Water
NO	Conservative chemical parameter, obtained as $NO = O_2 + R_N \cdot NO_3^-$
OMP	Optimum multiparameter analysis

POC	Particulate organic carbon
POM	Particulate organic matter
PON	Particulate organic nitrogen
R_N	Stoichiometric conversion factor of nitrate to dissolved oxygen, 9.3 mol O_2 mol NO_3^{-1}
SACW	South Atlantic Central Water
SACW_12	South Atlantic Central Water of 12ºC
SACW_18	South Atlantic Central Water of 18ºC
SE	Standard error
SPMW	Subpolar Mode Water
TDN	Total dissolved nitrogen
UNEADW	Upper North East Atlantic Deep Water

1. Introduction

The Eastern Boundary Upwelling Ecosystem (EBUE) associated with the Canary Current extends from the northern tip of the Iberian Peninsula at 43°N to South of Senegal at about 10°N (Arístegui et al., 2009). The intensity and persistence of upwelling-favourable winds increase with decreasing latitude, evolving from weak and seasonal to the North to strong and year-round to the South. The Canary Current EBUE is also characterized by an intense mesoscale activity in the form of upwelling filaments associated with prominent capes (Álvarez-Salgado et al., 2007; Lovecchio et al., 2018; Santana-Falcón et al., 2020) and island eddies (Barton et al., 1998; Sangrà et al., 2009; Cardoso et al., 2020). These mesoscale structures may export large amounts of organic matter produced over the shelf several hundreds of kilometres offshore (Gabric et al., 1993; Ohde et al., 2015; Lovecchio et al., 2018). Mesoscale activity is particularly intense in the southern boundary of the Canary Current EBUE due to the confluence of the Mauritanian upwelling and the Cape Verde Front (CVF). The CVF separates the eastern margins of the subtropical and tropical Atlantic gyres (Pelegrí and Peña-Izquierdo, 2015) and favours the horizontal transport from the coast, contributing to developing the giant filament of Cape Blanc (21ºN). This structure exports offshore massive amounts of biogenic organic matter produced in the Mauritanian coast (Van Camp et al., 1991; Gabric et al., 1993). At the CVF, Eastern North Atlantic Central Water (ENACW) encounters the slightly cooler, less saline, nutrient-richer and oxygen-poorer South Atlantic Central Water (SACW) (Zenk et al., 1991). In the frontal region, intense interleaving between the two water masses occurs (Pérez-Rodríguez et al., 2001; Martínez-Marrero et al., 2008), as well as the recurrent formation of meanders and eddies (Meunier et al., 2012; Alpers et al., 2013).

Upwelling filaments, meandering fronts and eddies affect the distribution and net community production of surface plankton communities in the Cape Verde Frontal Zone (CVFZ) (Olivar et al., 2016; Tiedemann et al., 2018; Arístegui et al., 2020). The organic matter transported by these structures is dominated by small suspended or slow sinking particulate organic matter, hereinafter suspended POM, and dissolved organic matter (DOM), while fast sinking POM (generally >100 μm) is less susceptible to horizontal advection (Álvarez-Salgado and Arístegui, 2015). Differentiation between suspended and sinking POM is of fundamental importance because of the contrasting mechanisms involved in their dispersion (horizontal export for suspended POM vs. vertical export for sinking POM) and fate during offshore transport from the coast to the ocean interior (Helmke et al., 2005; Fischer et al., 2009; Álvarez-Salgado and Arístegui, 2015). While suspended POM, is generally collected with Niskin bottles or stand-alone pumps, fast sinking POM is collected with sediment traps. POM is differentiated from DOM as the fraction of marine organic matter retained by a filter of a given pore size that usually range from 0.2 μm (polycarbonate, polysulfone, or aluminium filters) to 0.7 μm (typically glass fibber filters; Repeta, 2015). The CVFZ is characterized by the lateral export of organic matter from the coast to the open ocean not only in the surface nepheloid layer (SNL) but also in intermediate (INL) and bottom (BNL) nepheloid layers (Karakaş et al., 2006; Nowald et al., 2006; Fischer et al., 2009; Ohde et al., 2015), which affects carbon fluxes in the adjacent deep ocean waters (Alonso-González et al., 2009; Arístegui et al., 2020).

Information on the elemental composition of DOM, and suspended and sinking POM is crucial to understand the contrasting contribution of the three organic matter pools to the respiration in the ocean interior, which dictates the efficiency and magnitude of the biological carbon pump (Verdugo et al., 2004; Hopkinson and Vallino, 2005; Boyd et al., 2019). While an important effort has been made to characterize the origin, elemental composition and fluxes of sinking POM in the CVFZ (Helmke et al., 2005; Iversen et al., 2010; Álvarez-Salgado and Arístegui, 2015 and references therein; Fischer et al., 2019), the suspended POM and DOM fractions received much less attention (Alonso-González et al., 2009; Arístegui et al., 2020; Burgoa et al., 2020). Therefore the aim of this work is to study the dynamics of the dissolved and suspended fractions of organic matter in the CVFZ, and quantify the contribution of these pools to the remineralisation of organic matter in the dark ocean. Full-depth profiles of the carbon (C) and nitrogen (N) content

of DOM and suspended POM were obtained in a box (17-23ºN, 17-26ºW) that embraced the giant filament of Cape Blanc and the CVF. Differences in dissolved organic carbon (DOC) and suspended particulate organic carbon (POC) stocks, C:N molar ratios, and their relative contribution to dissolved oxygen consumption and nitrate production following organic matter mineralisation between transects (Northern, NACW domain; Southern, SACW domain; Eastern, Coastal Transition Zone domain; and Western, open ocean domain) are examined for the surface, central, intermediate and deep water masses present in the study area.

2. Materials and Methods

2.1. Sampling strategy

The FLUXES I cruise (R/V Sarmiento de Gamboa; Las Palmas - Las Palmas, 12 July to 9 August 2017) consisted of four transects (Northern, Western, Southern and Eastern) defining a box crossing the CVFZ, including 35 hydrographic stations 50 nautical miles apart (Figure 1). Three types of stations were occupied: short (nocturnal), medium (diurnal) and long (full day), which lasted 3, 9 and 27 hours, respectively (Figure 1). Medium and long stations were sampled from the surface to 4000 db, whereas short stations were sampled down to 2000 db. A rosette sampler carrying 24 Niskin bottles of 12 litres was used. It was equipped with a conductivity, temperature and depth (CTD) probe (SeaBird SBE911 plus), and sensors for dissolved oxygen (SeaBird SBE43), fluorescence of chlorophyll (SeaPoint SCF), and turbidity (SeaPoint STM). Sampling depths were selected based on the continuous records of the sensors attached to the rosette. Fifteen levels were sampled in medium and long stations (down to 4000 db) and 10 levels in short stations (down to 2000 db).

CTD conductivity was calibrated with water samples taken from the rosette and analysed on board with a Guildline 8410-A Portasal salinometer. Samples for dissolved oxygen (O_2) determination were analysed on board by the Winkler potentiometric method following the procedure described by Langdon (2010). The apparent oxygen utilization (AOU) was calculated with the equation of Benson & Krause, $AOU = O_{2sat} - O_2$ (UNESCO, 1986), where O_{2sat} is the dissolved oxygen saturation at local TS. The chlorophyll (Chl) fluorescence sensor was calibrated with water samples taken at 4 depths in the photic layer at each medium and long stations, where 500 mL of water was filtered and phytoplankton cells concentrated on 25 mm GF/F filters for chlorophyll a

determination. Pigments were extracted with 10 mL of 90% acetone at 4ºC in the dark for 24 h. The extracts were estimated fluorometrically by means of a Turner Designs bench fluorometer 10-AU, previously calibrated with pure chlorophyll a (Sigma Co.), as described in Holm-Hansen et al. (1965).

Water samples for the determination of inorganic nutrient concentrations were taken directly from the Niskin bottles in 25 mL polyethylene vials that were frozen at -20ºC until analysis in the base laboratory. A similar procedure was followed for dissolved organic carbon / total dissolved nitrogen (DOC / TDN) samples, which were collected in 30 mL amber glass vials with Teflon stoppers. Although these samples were not filtered, they will be named as DOC and TDN, because they mainly represent DOM due to the low concentrations of POM in oceanic waters. For the analysis of the concentration of suspended particulate organic carbon and nitrogen (POC and PON), 2 to 5 L of water were filtered onto pre-combusted (450ºC, 4 hours) 25 mm Whatman GF/F filters in a filtration system with a mild vacuum (pressure difference <300 mm Hg). Filters were transferred to 2 mL Eppendoff vials and dried for 12 hours in a vacuum desiccator with silica gel. After drying, they were frozen at -20ºC until analysis in the base laboratory. Dissolved oxygen, inorganic nutrients, DOC/TDN and POC/PON were collected at all stations and all sampling depths.

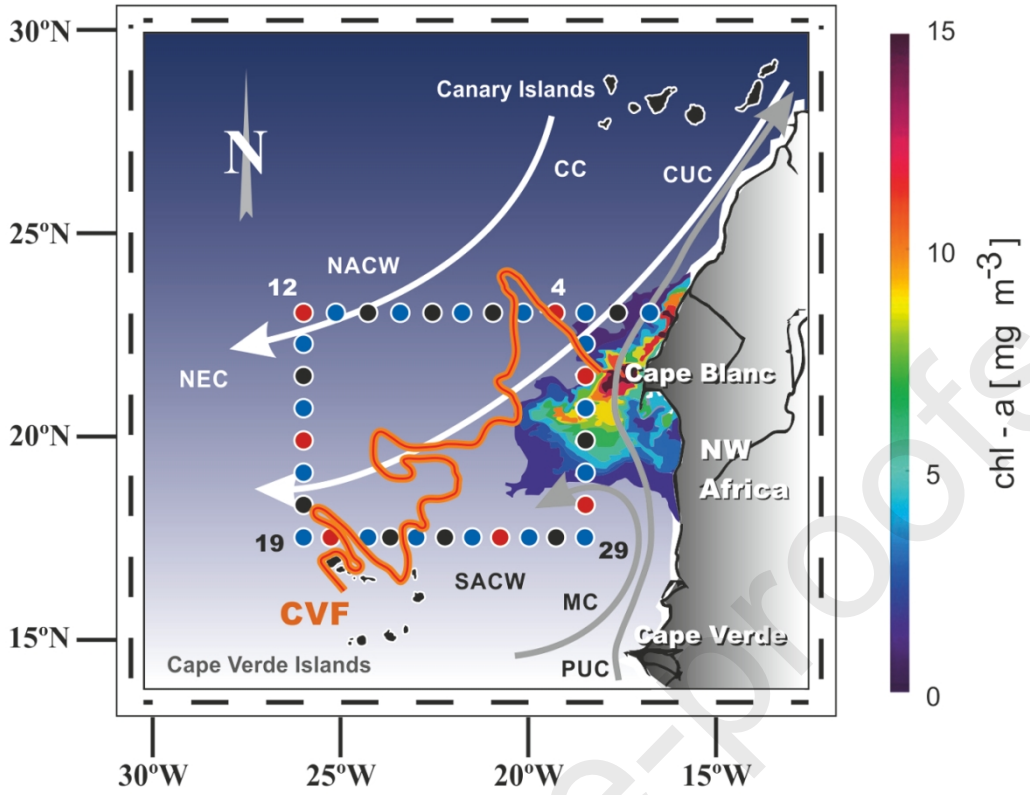

Figure 1. Map of the FLUXES I cruise. The dots represent the stations (blue: diurnal stations; black: nocturnal stations; red: long stations) the numbers indicate the station number, from 1 to 35. The main geographic and oceanographic features and currents are represented. The white arrows correspond to the Canary Current (CC), Canary Upwelling Current (CUC) and North Equatorial Current (NEC), the grey arrows to the Mauritania Current (MC) and the Poleward Undercurrent (PUC) (taken from Pelegrí and Peña-Izquierdo, 2015). The orange line represents the approximate position of the CVF during the cruise (taken from Burgoa et al. in review), and the colour contours near the coast represent the satellite chlorophyll *a* associated with the Cape Blanc filament on 24/07/2017 (from Copernicus Marine Service).

2.2. Analytical determinations

Micromolar concentrations of nutrient salts (nitrate, nitrite, ammonium, phosphate and silicate) were determined simultaneously by segmented flow analysis in an Alliance Futura autoanalyser following the methods of Hansen and Koroleff (1999) except for the case of ammonium, which was measured by the fluorometric method of Kérouel and Aminot (1997). Frozen samples were gently melted in the dark overnight and vigorously shaken before analytical determination.

The determination of suspended POC and PON in 25 mm GF/F filters was carried out by high temperature catalytic oxidation at 900ºC in a Perkin Elmer 2400 elemental analyser. At two selected stations, one from the Eastern (coastal) and one from the Western (open ocean) transects, the filters were divided into two parts; one part was measured directly and the other part was exposed to HCl fumes for 24 hours to remove

$CaCO_3$ before determination. After checking that $CaCO_3$ represented <10% of carbon in these filters, the rest of the filters were analysed directly. Therefore, although we have measured total carbon, we will refer to these measurements as POC because of the low levels of $CaCO_3$.

DOC and TDN were analysed by high temperature catalytic oxidation at 680ºC with a Shimadzu TOC-V analyser connected in line with a TNM1 measuring unit. After melting, the samples were acidified to pH <2 and degassed with high purity N_2 to eliminate the CO_2 before measurement. Aliquots of 150 µL were injected in the analyser. Measurements were made in triplicate to quintuplicate. The accuracy was checked daily with the DOC/TDN reference materials (CRM) provided by D.A. Hansell (University of Miami, USA). Measured concentrations of the CRM were 44.9 ± 1.7 µmol C L^{-1} (n = 10) and 31.7 ± 1.4 µmol N L^{-1} (n = 10); the certified values are 43–45 µmol C L^{-1} and 32–33 µmol N L^{-1} (DSW Batch 16–2016*Lot 05-16). DON concentrations were calculated as DON = TDN - DIN where DIN is the dissolved inorganic nitrogen (nitrate + nitrite + ammonium).

2.3. Water mass analysis

An optimum multiparameter (OMP) inverse method (Karstensen and Tomczak, 1998) has been used for the quantification of the water types (WTs) that contribute to the water samples collected in the CVFZ during FLUXES I. A water type (WT) is a body of water formed in a particular region of the ocean with certain thermohaline and chemical properties (Tomczak, 1999).

In our OMP, the variables used to define the WTs were potential temperature (θ), salinity (S), silicate (SiO_4H_4) and the conservative chemical parameter NO ($NO = O_2 + R_N \cdot NO_3^-$ (Broecker, 1974) where R_N was set to a constant value of 9.3 mol O_2 mol NO_3^- [1] (Anderson, 1995)), and represents the Redfield ratio of dissolved oxygen consumption to nitrate production during the mineralisation of biogenic organic matter in the ocean. We identified 11 WT in the CVFZ: Madeira Mode Water (MMW); Eastern North Atlantic Central Water (ENACW) of 15ºC and 12ºC; South Atlantic Central Water of 18ºC and 12ºC; Subpolar Mode Water (SPMW); Antarctic Intermediate Water (AA); Mediterranean Water (MW); Labrador Sea Water (LSW); and upper and lower North East Atlantic Deep Water (NEADW). The physical and chemical properties of most of

these WTs were obtained from the literature (Table 1), except for AA and SACW of 18ºC and 12ºC, which were defined from the average characteristics of these WTs in the Eastern Equatorial Atlantic, between 5º N–5º S and 20–30º W (World Ocean Atlas, 2013). This source region was chosen because AA and SACW are transported from the Equatorial Atlantic to the CVFZ by the Mauritanian current (Figure 1). The in situ values of θ, S, SiO_4H_4 and NO from the rosette sampler profiles collected during the cruise were used to calculate the contribution of each WT to every sample, by solving this set of mass balance equations per sample:

$$\sum_i X_{ij} \cdot \theta_i = \theta_j + R\theta_j$$

$$\sum_i X_{ij} \cdot S_i = S_j + RS_j$$

$$\sum_i X_{ij} \cdot (SiO_4H_4)_i = (SiO_4H_4)_j + R(SiO_4H_4)_j$$

$$\sum_i X_{ij} \cdot NO_i = NO_j + RNO_j$$

$$\sum_i X_{ij} = 1 + R\sum$$

Where the subscript i corresponds to each WT and j to every sample; X_{ij} are the proportion of water type i in sample j; θ_i, S_i, $(SiO_4H_4)_i$ and NO_i are the WT i values of θ, S, SiO_4H_4 and NO; and θ_j, S_j, $(SiO_4H_4)_j$ and NO_j are the values for each variable in sample j; R are the residuals each the mass balance equations and for the mass conservation equation for sample j.

These linear mixing equations were normalized and weighted. For normalization, the mean and standard deviation values of the parameters in Table 1 were used. The equations were weighted considering the measurement error of each parameter in relation to its variability in the study area and its relative conservative nature. Weights of 10, 10, 2 and 1 were assigned to θ, S, NO and SiO_4H_4, respectively. The weights assigned to the NO and SiO_4H_4 mass balance equations were lower because both variables are affected by non conservative processes: SiO_4H_4 is influenced by silica dissolution and the R_N of NO is variable, which introduces more uncertainty in the mass balance equations. We

assumed that the mass is accurately conserved, so a weight of 100 was assigned to the mass conservation equation.

Since we have 5 mass balance equations and 11 WTs, in order to solve the OMP it is necessary to define oceanographically consistent WT mixing groups, taking into account that mixing occurs with adjacent WTs along or across isopycnals and a maximum of 4 WTs can mix simultaneously (Álvarez et al., 2014). The 5 groups of WTs defined, from surface to 4000 db were: 1) MMW - SACW18 - ENACW15; 2) SACW18 - ENACW15 - SACW12 - ENACW12; 3) SACW12 - ENACW12 - SPMW - AA; 4) SPMW - AA - MW - LSW; and 5) MW - LSW - LNEADW - UNEADW (Figure 2). Each sample was assigned to a particular group according to its θ and S, and then the system of mass balance equations was solved for each sample.

The reliability of the OMP analysis was assessed with the determination coefficient (R^2) and standard error (SE) of the residuals of the linear regression between measured and back-calculated variables (θ, S, SiO_4H_4 and NO) (Álvarez et al., 2014). Note that our OMP reproduced the thermohaline and chemical fields during the cruise quite accurately, as demonstrated by the high R^2 (>0.977) and low SE of the linear regression of the measured and predicted values of θ, S, SiO_4H_4 and NO (Table 1).

Samples located between the surface and the base of the deep chlorophyll maximum (DCM) were excluded from the OMP analysis because the heat, freshwater and gas exchange with the atmosphere and the non conservative behaviour of O_2 and nutrient salts would disprove the assumption of conservation of the mass balance equations. Therefore, the OMP was applied to 307 of the 419 samples in which DOC, DON, PON and POC were determined.

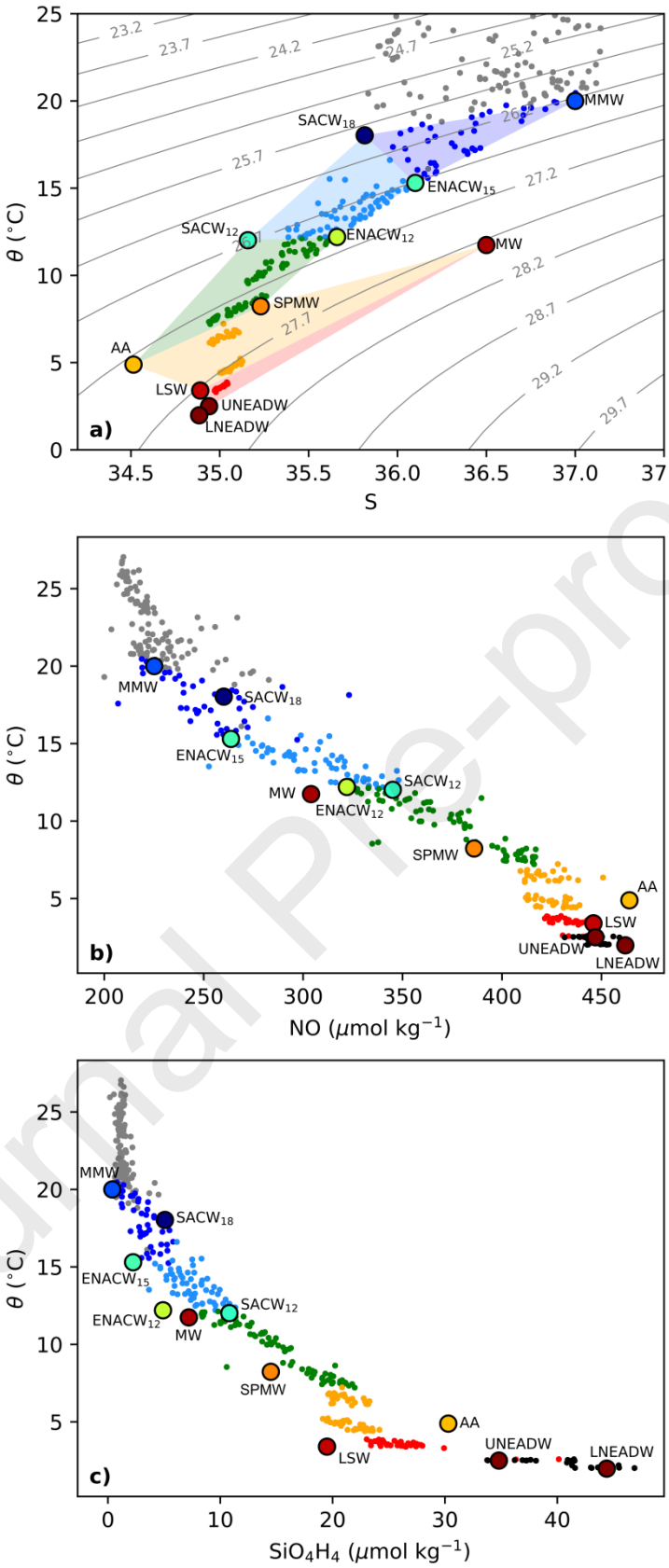

Figure 2. Potential temperature (θ) versus salinity (a), NO (b) and SiO_4H_4 (c) for FLUXES I. Dots represent the water samples collected and the shading colours in (a) identify the mixing group assigned to each sample. Potential density contours are also shown in (a).

Table 1.Thermohaline and chemical characteristics (average value ± uncertainty) of the water types (WT) introduced in the OMP analysis of the water masses present in the CVFZ. Determination coefficient (R^2), standard error (SE) of the estimate and number of samples (n) of the multiple-regression of the measured and back-calculated variables.

WT	θ_i (ºC)	S_i	SiO_4H_{4i} (µmol kg^{-1})	NO_i (µmol kg^{-1})
SACW_18 [a]	18.03 ± 0.05	35.82 ± 0.03	5.1 ± 0.1	260 ± 8
MMW [b]	20.0 ± 0.5	37.00 ± 0.04	0.4 ± 0.3	225 ± 10
ENACW_15 [b]	15.3 ± 0.4	36.10 ± 0.02	2.2 ± 1.7	264 ± 8
SACW_12 [a]	12.0 ± 0.1	35.16 ± 0.01	10.8 ± 0.1	345 ± 7
ENACW_12 [c]	12.2 ± 0.4	35.66 ± 0.02	4.9 ± 0.2	322 ± 8
SPMW [c]	8.2 ± 0.4	35.23 ± 0.01	14.5 ± 0.4	386 ± 7
AA [a]	4.89 ± 0.03	34.51 ± 0.02	30.3 ± 0.8	464 ± 8
MW [c]	11.8 ± 0.1	36.50 ± 0.01	7.2 ± 0.7	304 ± 9
LSW [c]	3.4 ± 0.2	34.89 ± 0.12	19.5 ± 0.4	446 ± 9
UNEADW [d]	2.500 ± 0.003	34.940 ± 0.003	34.8 ± 0.3	447 ± 7
LNEADW [d]	1.980 ± 0.002	34.884 ± 0.003	44.4 ± 0.3	462 ± 7
R^2	0.999	0.999	0.988	0.977
SE	0.04	0.005	1.2	11
N	307	307	307	307

[a] This work, taken from the WOA13 in the Equatorial Atlantic
[b] Álvarez and Álvarez-Salgado (2009); Lonborg & Álvarez-Salgado (2014)
[c] Perez et al. (2001); Álvarez and Álvarez-Salgado (2009)
[d] Perez et al. (2001); Lonborg & Álvarez-Salgado (2014)

2.4. WT proportion-weighted average values

The WT proportion-weighted average value of any variable (N) in a given WT, henceforward archetype concentration of N, can be calculated using the X_{ij} obtained as detailed in section 2.3, and the concentration of N in each sample (Álvarez-Salgado et al., 2013). The equation is:

$$N_i = \frac{\sum_j X_{ij} \cdot N_j}{\sum_j X_{ij}}$$

Where N_i is the archetype value of N in water mass i; X_{ij} is the proportion of WT i in sample j and N_j is the value of N in sample j. The standard error of the archetype value is obtained as:

$$SE_{N_i} = \frac{\sqrt{\sum_j X_{ij} (N_j - N_i)^2}}{\sum_j X_{ij}}$$

Finally, the proportion of the total volume of water sampled during the cruise that correspond to a given water mass (%VOL_i) can be calculated as:

$$\%\mathrm{VOL}_i = 100 \cdot \frac{\sum_j X_{ij}}{n}$$

Where *n* is number of samples. In this study, we have calculated archetype values of Z, S, θ, AOU, DOC, DON, POC and PON for the 11 WTs identified in the study area. Moreover, N_i values were calculated also for the Northern (stns 3 to 12, excluding stations 1 and 2 over the continental shelf) and Southern transects (stns 19 to 29) -separated by the CVF- and the Western transect (stns 12 to 19) -located in the open ocean- and the Eastern transect (stns 29 to 35 and stn 3) near the coast (Figure 1), to assess geographical differences between transects within a given WT.

2.5. Multiple regression models

The fraction of the total variability of the distribution of a non-conservative variable (e.g. DOC, DON, POC, PON) explained by WT mixing can be calculated from a multiple linear regression of the non-conservative variable with the water mass proportions:

$$N_j = \sum_j X_{ij} \cdot n_i$$

Where N_j is the concentration of the non-conservative variable, with j = 1… n (one per sample) and n_i is the correlation coefficient of WT i, with i = 1… m (one per WT). The per cent of explained variability is indicated by the determination coefficient (R^2) and the explanatory power by the standard error of the estimate (SE) of the multiple regression.

However, the distributions of DOC, DON, POC or PON depend not only on the conservative mixing of WTs but also on the biogeochemical processes that occur alongside mixing. The main biogeochemical process in the ocean interior is organic matter mineralisation and it can be traced with AOU (Álvarez et al., 2014). The observed organic matter mineralisation is the result of the large-scale mineralisation from the formation area of each WT to the study area and the local mineralisation that occurs within the study area (Álvarez-Salgado et al., 2013; Álvarez et al., 2014), the CVFZ in our case. On the one hand, the large-scale mineralisation is assumed to be included in the

archetype value of each WT and, therefore, accounted for by the multiple linear regression with X_{ij}. On the other hand, a multiple linear regression with X_{ij} and AOU (for DOC, DON, POC and PON) or NO_3^- (for DON and PON) would quantify the local mineralisation of DOM and suspended POM:

$$N_j = \sum_j X_{ij} \cdot n_i + \beta \cdot AOU\ (or\ NO_3^-)$$

In this multiple linear regression of n linear equations with m + 1 unknowns, the extra unknown (β) is the coefficient that relates DOC, DON, POC or PON with AOU or NO_3^- and represents the rate of change of DOM and suspended POM with AOU or NO_3^- that does not depend on WT mixing (Álvarez-Salgado et al., 2013). Therefore, when calculating the multiple linear regression of DON or PON with X_{ij} and NO_3^-, the coefficient β would represent the contribution of DON or PON to the local NO_3^- production by organic matter mineralisation. On the other hand, the coefficient β in the multiple linear regression of DOC or POC to AOU would represent the contribution of DOC or POC to the oxygen utilisation. In this case, once β is multiplied by the Redfield ratio of dissolved oxygen consumption to organic carbon mineralisation of 1.4 mol O_2 mol C^{-1} (Anderson, 1995), it would represent the contribution of DOC or POC to the local production of inorganic nitrogen by organic matter mineralisation. Finally, once the contribution of DOM and suspended POM to organic matter mineralisation is calculated from β, the contribution of sinking POM can be estimated indirectly by difference.

2.6. Epipelagic layer

As indicated above, samples collected in the epipelagic layer were excluded from the OMP analysis because of the non-conservative behaviour of θ, S, SiO_4H_4 and NO. Those samples have been used to study the impact of the CVFZ on the biogeochemistry of the epipelagic layer during the FLUXES I cruise. To do that, we have calculated average concentrations of the different variables (Z, S, θ, AOU, Chl-a, NO_2^-, NO_3^-, NH_4^+, DOC, DON, POC and PON) at the surface (5 db), and the deep chlorophyll maximum (DCM), as well as vertically-averaged from the surface to the base of the DCM. Vertical averages considered the uneven vertical sampling spacing by using the trapezoid rule to weight each sample. The average values were obtained for the whole cruise as well as for each individual transect. In the Northern transect, the first two stations were excluded

because they are outside the box, and due to their position close to the continental shelf, they are affected by distinct processes from those observed in the oceanic waters, biasing the calculation of the average values of the Northern transect (Figure 1).

3. Results

3.1. Hydrographic setting of the CVFZ

3.1.1 Epipelagic waters

The relative position of the four transects with respect to the CVF during FLUXES I can be documented using the isohaline that defines the front (36 at 150 db) (Zenk et al., 1991) (Figure 3a). According to this criterion, the Western and Northern transects were located to the North of the front, while the front intersected the Southern and Eastern transects around stations 34 and 24, respectively (Figure 1). Due to the dominance of saline waters of North Atlantic origin to the North of the front, the average salinity was significantly higher in the Northern and Western transects (36.7-36.8), than in the Southern and Eastern transects (36.2) (Figure 3a, Table S1). Mesoscale variability was super-imposed over this large-scale pattern, notably due to the presence of a narrow intrusion of relatively cold and less saline water of South Atlantic origin centred at stn 5 in the Northern transect. The mean depth-averaged temperature down to the base of the DCM was 22.3ºC with non-significant differences between transects (Figure 3b, Table S1). Nonetheless, the Southern transect was characterized by significantly higher ($p < 0.0005$) surface (5 db) temperatures (26.1ºC) than the Northern transect (23.9ºC).

The DCM was shallower and with higher Chl-a levels towards the coast (Figure 3c). The average depth of the DCM and average Chl-a levels in the Northern and Southern transect, were similar ($p > 0.3$) while the Western (oceanic) and Eastern (coastal) transects showed the highest differences, being the DCM deeper and with lower concentrations in the Western transect (Table S1).

The distribution of AOU (Figure 3d) matched the predominant form of inorganic nitrogen, NO_3^- (Figure 4a), increasing significantly with depth (Table S1). In the same way as salinity and temperature, marked differences were observed between the Northern and Southern transects of the CVF: depth-averaged concentrations of AOU and NO_3^- were significantly lower ($p < 0.05$) in the Northern and Western transects (<4.5 and <2.3

μmol kg^{-1}, AOU and NO_3^- respectively) than in the Southern and Eastern transects (>20 and >4.6 μmol kg^{-1}, respectively). The intrusion of water with South Atlantic origin at stn 5 is traced by higher AOU and NO_3^- values in the upper 100 db (Figures 3d, 4a).

NH_4^+ (Figure 4b) and NO_2^- (Figure 4c) were, in general, very low (<0.06 and <0.14 μmol kg^{-1}), except in the surroundings of the DCM. An average NH_4^+ concentration of 0.09 ± 0.03 μmol kg^{-1} was observed at the DCM, with significantly ($p < 0.01$) lower values (0.02 ± 0.03 μmol kg^{-1}) in the Western (oceanic) transect and higher values (0.19 ± 0.10 μmol kg^{-1}) in the Eastern (coastal) transect. The average concentration of NO_2^- at the DCM was 0.23 ± 0.03 μmol kg^{-1}, being also significantly lower in the Western transect ($p < 0.025$).

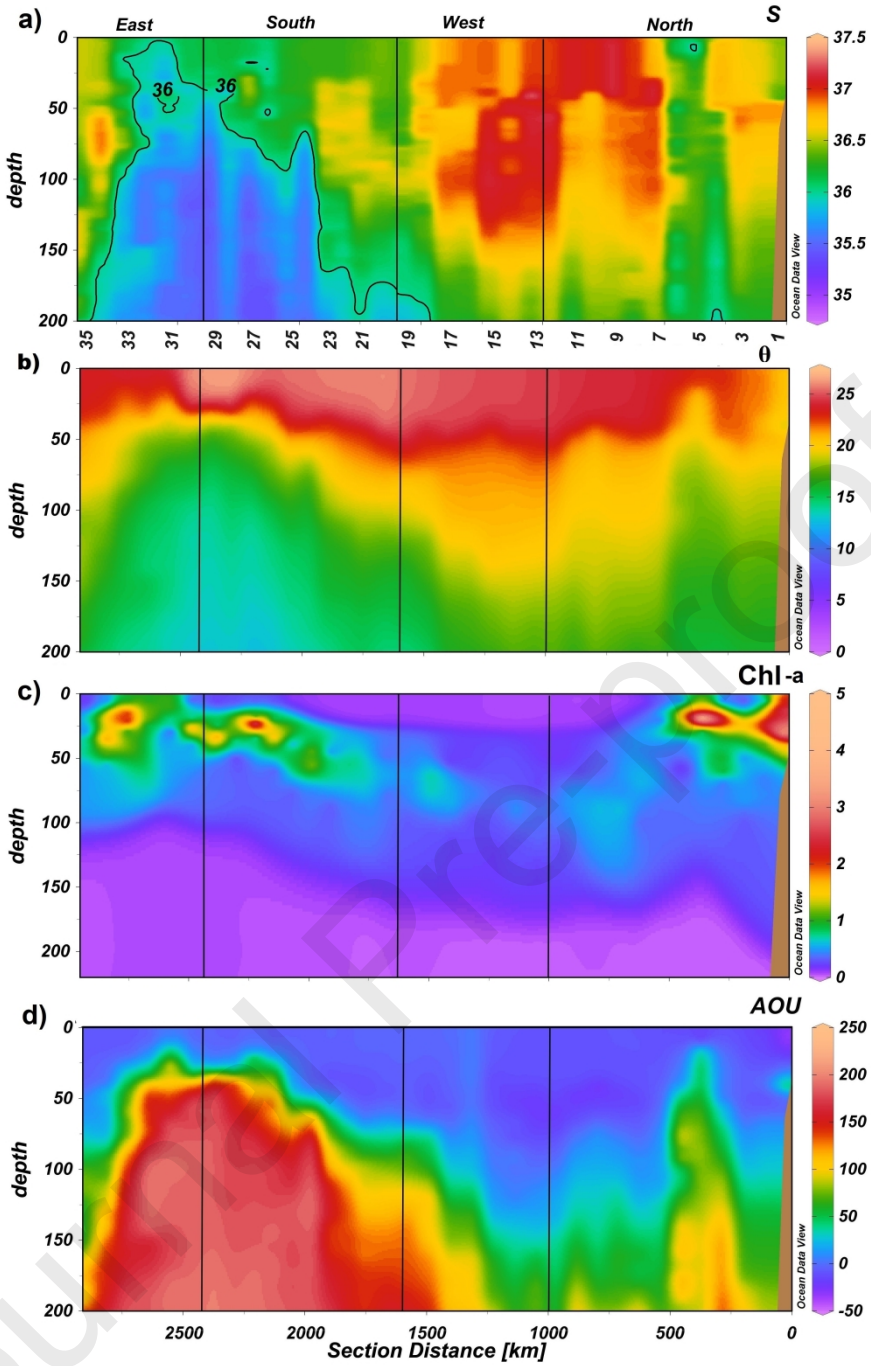

Figure 3. Distribution of salinity (S) (a), potential temperature (θ) in °C (b), Chl (chlorophyll a) in µg L^{-1} (c) and apparent oxygen utilization (AOU) in µmol kg^{-1} (d), in the epipelagic layer during the FLUXES I cruise. The black line in (a) represents the 36 isohaline defining the location of the CVF, and the vertical black lines represent the corners of the FLUXES hydrographic box. The y-axis can be read as station number (a) or section distance (d). Produced with Ocean Data View (Schlitzer, 2017).

NH_4^+ and NO_2^- also showed relatively elevated concentrations at stn 5 in the Northern transect, coinciding with the relative maxima in temperature, Chl-a, AOU and NO_3^-, and minimum in salinity, reflecting the influence of the mesoscale variability of the CVF in the distribution of biogeochemical properties.

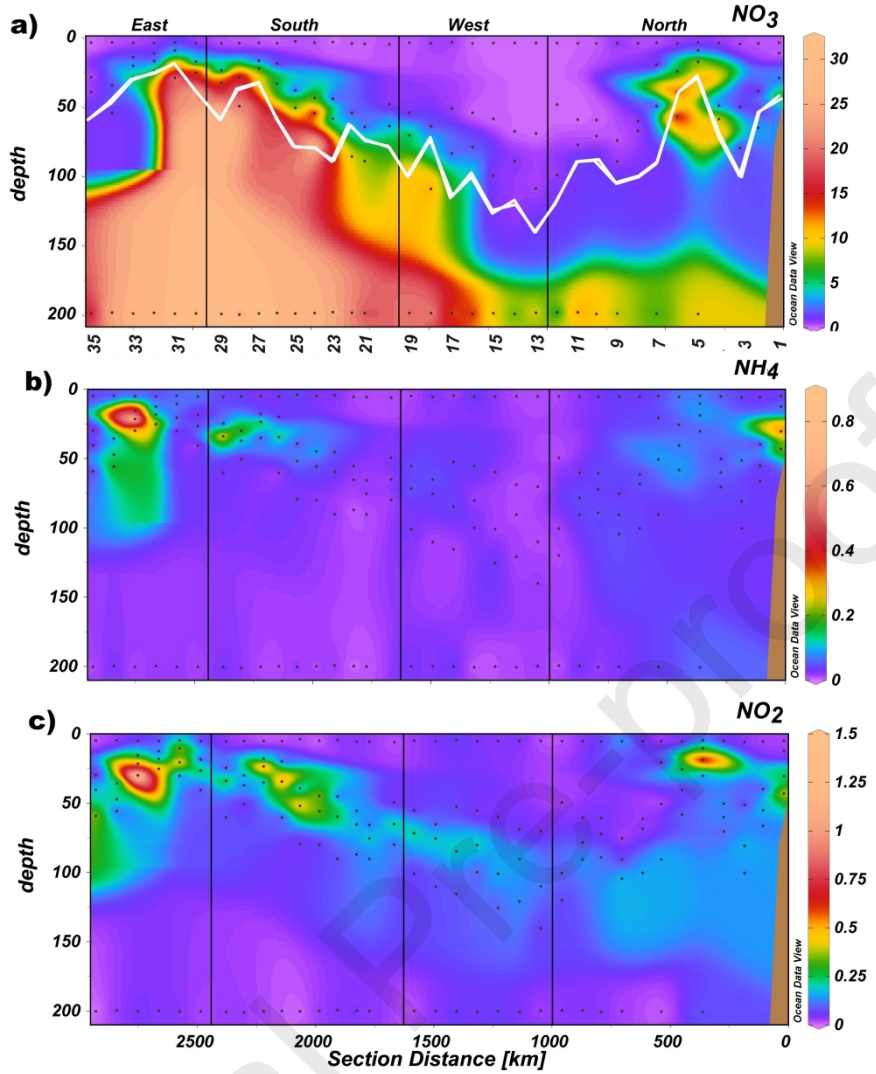

Figure 4. Distributions of nitrate (NO_3^-) in µmol kg^{-1} (d) (a), ammonium (NH_4) in µmol kg^{-1} (b), and nitrite (NO_2^-) in µmol kg^{-1} (c), in the epipelagic layer during the FLUXES I cruise. Dots represent samples, vertical back lines represent the corners of the FLUXES I hydrographic box and the white line in panel a represents the base of the DCM. The y-axis can be read as station number (a) or section distance (c). Produced with Ocean Data View (Schlitzer, 2017).

3.1.2. Meso- and bathypelagic waters

Below the epipelagic layer, in the depth range between 100-700 db, hydrographic variability was governed by the distribution of the central water types. SACW_18 and MMW, characterized by potential temperatures of 18ºC and 20ºC, respectively (Table 1, Figures 5ab, S1a), and centred at about 110 db (Table 2) were the shallowest central water types. SACW_18 and MMW were defined by distinct salinity values, 35.82 and 37.00, respectively (Table 1, Figures 5ab, S1b), as expected for two water masses of contrasting North and South Atlantic origin, and represented 4.78% and 5.48% of the total sampled water volume (Table 2) or 9.9% an 11.4% of the volume of central waters. ENACW_15 was located deeper, centred at 240 ± 14 db (Table 2) and represented 12.54% of the total

sampled volume or 26.1% of the volume of central waters. Most of the ENACW_15 was present in the Northern and Western transects (42.8% and 25.0% of the volume of this WT, respectively), i.e. to the North of the CVF (Figure 5c). SACW_12 and ENACW_12 were centred at 336 ± 28 db and 442 ± 19 db and were defined by a similar temperature of ~12ºC, but different values of salinity (35.16 and 35.66), SiO_4H_4 (10.8 and 4.9 µmol kg^{-1}) and NO (345 and 322 µmol kg^{-1}) (Table 1). ENACW_12 was the most abundant WT sampled during the cruise with 18.09% (Table 2, Figure 5b) or 37.6% of the volume of central waters and was present in the four transects (from a minimum of 17.8% of the total volume in the Western transect to a maximum of 28.6% in the Northern transect). Conversely, SACW_12 occupied a volume of 7.25% (or 15.1% of the central waters) and was mostly present in the stations of the Southern transect, where 57% of the volume of this WT was found (Table 2, Figure 5a). Again, in the Northern section, around stn 5, SACW_18 appears, although ENACW dominated in the rest of the transect (Figure 5).

The intermediate water domain, approximately between 700 db and 1500 db, was occupied by AA, SPMW and MW. These water masses, of contrasting sub-Antarctic, sub-Arctic and Mediterranean origin, have remarkable differences in θ, S, SiO_4H_4 and NO (Table 1). It is particularly noticeable the salinity minimum observed in the Southern transect at about 1000 db, which corresponds to AA (Figures 5c, S1b). The shallowest intermediate WT was the SPMW, centred at 809 ± 32 db, with a temperature of 8ºC and representing 7.18% of the sampled volume (or 34.3% of the intermediate waters).

SPWM was followed by AA at a depth of 873 ± 54 db, which had the lowest salinity 34.52 but the highest content of silicates 30.3 µmol kg^{-1} and occupied a volume of 10.62% (or 50.8% of the intermediate waters). This water mass was mostly present to the South of the CVF (59.0% of the volume sampled in the Northern and Western transects) while SPMW predominated to the North of the front (56.8% of the sampled volume in the Eastern and Southern transects) (Figure 5d). The deepest intermediate WT, MW, centred at 1455 ± 118 db, was much less represented with 3.09% (14.8% of the intermediate waters) and was almost absent in the Eastern transect (only 3.1% of the volume).

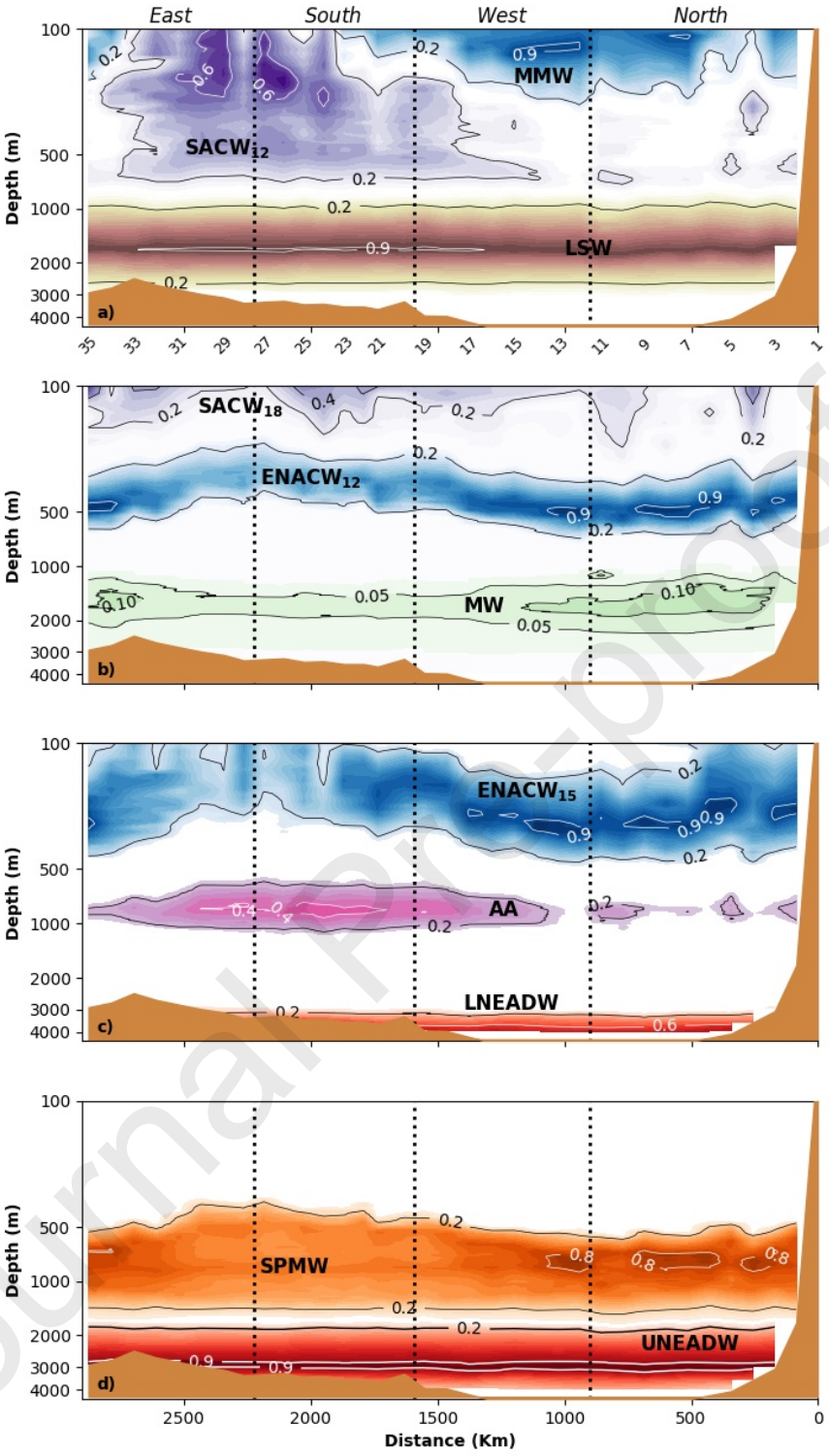

Figure 5. Distributions of the water masses described in the CVFZ during the FLUXES I cruise. Vertical black lines represent the corners of the FLUXES I hydrographic box. Water mass proportions in this figure were derived with an OMP analysis applied to CTD data at 1 db vertical resolution. θ and S were measured directly with the CTD, while SiO_4H_4 and NO values were reconstructed by fitting the measured water sample concentrations to a non-linear combination of variables directly measured with the CTD (θ, S, O_2) (Figures S1 and S2). The distribution of the water-masses among the panels was designed to avoid contour overlapping and does not follow an oceanographic criteria. The y-axis can be read as station number (a) or section distance in km (d).

Table 2. Percentage of the total volume of water sampled during FLUXES I that corresponded to each water type (%VOLi) and archetype values ± SE of depth (Zi), apparent oxygen utilization (AOUi), nitrate (NO_3^- i), dissolved organic carbon (DOCi), dissolved organic nitrogen (DONi), particulate organic carbon (POCi), particulate organic nitrogen (PONi), and C:N ratios of DOM and suspended POM for the water types intercepted during the cruise. Determination coefficient (R^2), standard error of the estimate (SE) of the multiple-regression of each variable with the water type proportions X_{ij}.

WT	%VOLi	Zi (db)	AOUi (µmol kg^{-1})	NO_3^{-1}i (µmol kg^{-1})	DOCi (µmol L^{-1})	DONi (µmol L^{-1})
SACW_18	4.78%	102 ± 19	120.2 ± 15.4	16.9 ± 2.1	58.9 ± 2.5	4.6 ± 0.4
MMW	5.48%	113 ± 3	50.9 ± 10. 5	6.5 ± 1.4	58.7 ± 1.6	5.1 ± 0.3
ENACW_15	12.54%	240 ± 14	117.8 ± 6.7	16.2 ± 1.0	52.3 ± 1.7	4.2 ± 0.3
SACW_12	7.25%	336 ± 28	191.7 ± 5.4	28.7 ± 1.0	49.9 ± 1.5	3.5 ± 0.3
ENACW_12	18.09%	442 ± 19	171.2 ± 4.8	27.2 ± 0.8	48.5 ± 0.6	3.4 ± 0.2
SPMW	7.18%	809 ± 32	175.7 ± 4.2	30.9 ± 0.7	44.8 ± 0.6	3.3 ± 0.3
AA	10.62%	873 ± 54	172.6 ± 5.7	31.3 ± 0.6	45.1 ± 0.6	3.1 ± 0.3
MW	3.09%	1455 ± 118	119.4 ± 9.2	25.9 ± 1.2	43.3 ± 0.9	3.0 ± 0.4
LSW	15.58%	1688 ± 46	104.0 ± 2.6	23.9 ± 0.3	43.4 ± 0.5	3.0 ± 0.2
UNEADW	11.72%	2742 ± 93	88.0 ± 1.1	22.2 ± 0.2	43.4 ± 0.6	2.9 ± 0.2
LNEADW	3.66%	3824 ± 101	85.1 ± 1.7	22.4 ± 0.2	43.5 ± 1	3.1 ± 0.3
R^2			0.94	0.95	0.63	0.44
SE			12.9	1.8	4.0	0.9

WT	POCi (µmol L^{-1})	PONi (µmol L^{-1})	C:N DOM (mol C mol N^{-1})	C:N POM (mol C mol N^{-1})
SACW_18	3.2 ± 1.2	0.33 ± 0.13	12.7 ± 1.1	9.9 ± 1.6
MMW	2.7 ± 1.0	0.25 ± 0.10	11.6 ± 0.7	10.9 ± 1.3
ENACW_15	1.5 ± 0.3	0.12 ± 0.03	12.4 ± 1.0	12.3 ± 0.9
SACW_12	1.4 ± 0.2	0.11 ± 0.02	14.4 ± 1.5	12.4 ± 1.4
ENACW_12	1.2 ± 0.1	0.09 ± 0.01	14.4 ± 1.1	12.5 ± 0.8
SPMW	0.79 ± 0.06	0.05 ± 0.01	13.6 ± 1.3	14.5 ± 1.3
AA	0.81 ± 0.06	0.06 ± 0.01	14.6 ± 1.3	14.2 ± 1.3
MW	0.70 ± 0.11	0.05 ± 0.01	14.4 ± 1.9	14.2 ± 2.2
LSW	0.67 ± 0.05	0.05 ± 0.01	14.5 ± 0.9	14.6 ± 1.1
UNEADW	0.68 ± 0.07	0.04 ± 0.01	15.2 ± 0.9	15.6 ± 1.3
LNEADW	0.71 ± 0.12	0.04 ± 0.01	14.8 ± 1.5	17.3 ± 2.0
R^2	0.26	0.29		
SE	1.3	0.13		

Finally, the deep waters domain was composed by three water types with similar salinity, yet different silicate content (Figure S1c) due to their contrasting origin. While LSW is of pure North Atlantic origin, LNEADW and UNEADW are mixed with Antarctic waters that confer their higher silicate concentration. LSW was defined by a

silicate concentration of 19.5 µmol kg^{-1}, it was located at 1648 ± 46 db and represented 15.58% of the sampled volume (50.3% of the deep waters), being the second predominant water mass sampled during FLUXES I. LSW was found in the four transects, ranging from 19.9% of the total volume in the Eastern transect to 29.4% in the Northern transect (Figure 5a). In contrast, UNEADW was located deeper at 2742 ± 93 db and had a silicate concentration of 34.8 µmol kg^{-1}, with a volume sampled of 11.72% (37.9% of the deep waters). LNEADW was placed at 3824 ± 101 db, with a silicate concentration of 44.4 µmol kg^{-1} and a small representation of sampled volume of 3.66% (or 11.8% of deep waters). UNEADW was distributed in the four transects, ranging from 18.7% of the total volume in the Eastern transect to 29.0% in the Southern transect (Figure 5d). In contrast, LNEADW concentrated in the Northern and Western transects (75% of the total volume of this WT) while it was practically absent in the Eastern transect. Bottom depth is the likely reason behind this difference (Figure 5c).

3.2. Biogeochemical variability in epipelagic, meso- and bathypelagic waters of the CVFZ

3.2.1 Organic matter variability in epipelagic waters

DOC (Figure 6a) and DON (Figure 6b) showed maximum average concentrations of 80.9 ± 1.7 µmol L^{-1} and 6.7 ± 0.2 µmol L^{-1} at the surface layer (Table S1), and decreased with depth. At the surface, DOC and DON levels were significantly higher in the Southern transect, while at the DCM, the highest DOC and DON concentrations were found in the Eastern (coastal) transect (Table S1, Figure 6a,b). The average C:N molar ratio of DOM throughout the epipelagic layer was 12.0 ± 0.3 and showed similar values in all transects at the surface and the DCM ($p > 0.05$).

POC (Figure 6c) and PON (Figure 6d) concentrations showed similar distributions with a marked decrease below the DCM. Maximum concentrations of POC and PON were observed at the stations near the coast, in the Northern and Eastern transects.

Maximum POC coincided with the DCM in the Eastern (10.4 ± 2.0 µmol L^{-1}) transect, in the Western (2.8 ± 0.3 µmol L^{-1}) transect it was located at the surface, while in the Northern (6.9 ± 2.1 µmol L^{-1}) and Southern (5.7 ± 1.1 µmol L^{-1}) transects it was somewhat above the DCM. Maximum PON concentrations followed the same pattern

(Figure 6d). In the upper 50 db, stn 5 shows very high values of DOC, DON, POC and PON.

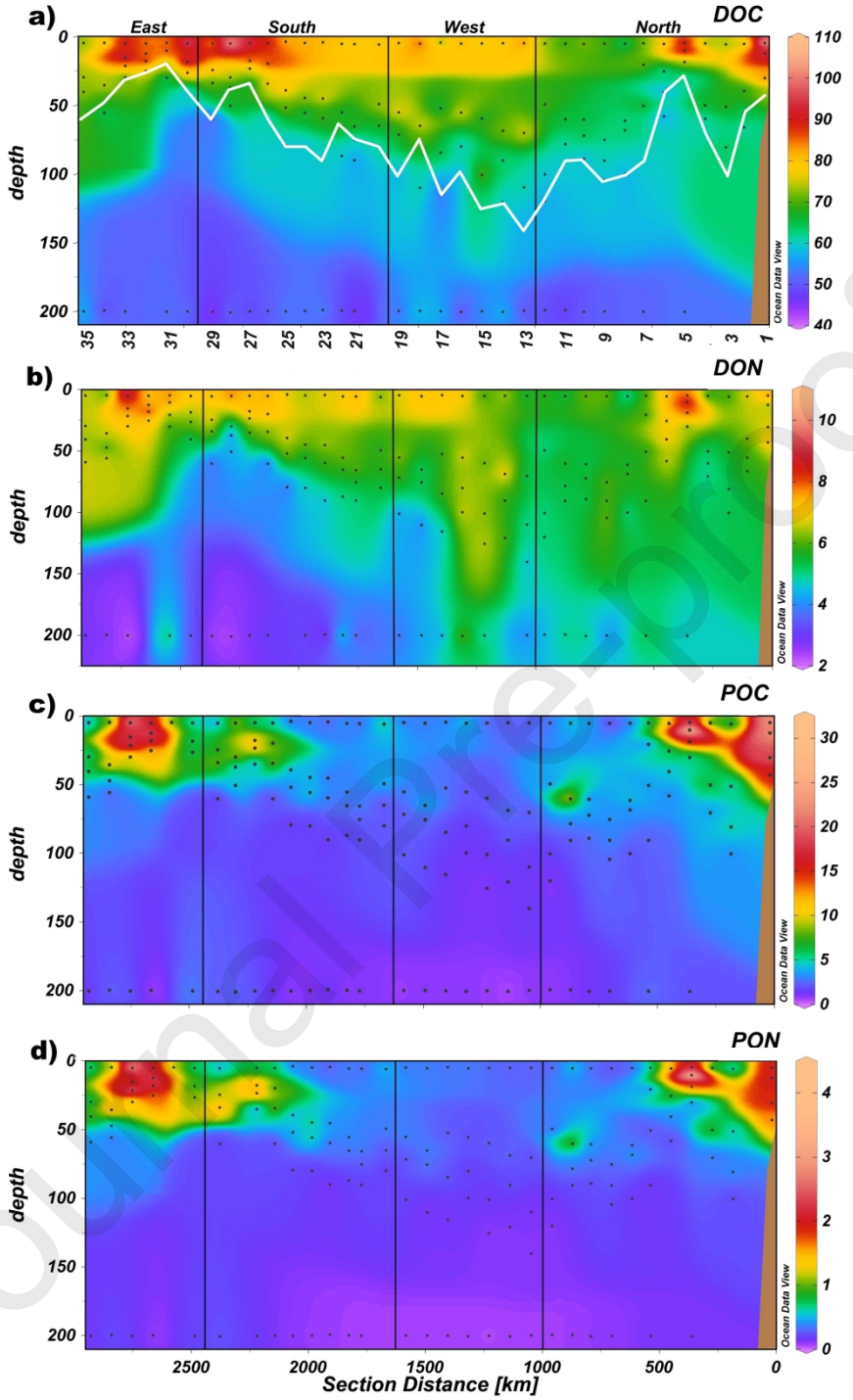

Figure 6. Distributions of DOC in µmol L^{-1} (a), DON in µmol L^{-1} (b), POC in µmol L^{-1} (c) and PON in µmol L^{-1} (d) in the epipelagic layer during the FLUXES I cruise, dots represent samples, vertical black lines represent the corners of the FLUXES I hydrographic box, and the white line in a) represent the base of DCM. The y-axis can be read as station number (a) or section distance in km (d). Produced with Ocean Data View (Schlitzer, 2017).

The average value of the C:N molar ratio of POM over the epipelagic layer, 8.1 ± 0.4, was significantly lower than the average C:N molar ratio of DOM, 12.0 ± 0.3 (Table S1). Average C:N ratios of POM were significantly higher in the Northern and Western transects (>8.9) than in the Southern and Eastern transects (<7.3) ($p < 0.005$). In the Western, Southern and Eastern transects, minimum values of the C:N ratio of POM were associated with the DCM as for the case of the C:N ratio of DOM (Table S1).

3.2.2 Organic matter variability in meso- and bathypelagic waters

AOU can be used to trace organic matter mineralisation in the meso- and bathypelagic layers of the CVFZ (Figure 7a). In the central waters, the lowest archetype AOU values (50 to 120 µmol kg^{-1}) were found in the shallowest WTs (MMW, ENACW_15 and SACW_18), while the highest archetype AOU (192 µmol kg^{-1}) corresponded to SACW_12 (Table 2). In intermediate and deep waters, AOU decreased significantly ($p < 0.0005$) with depth from an archetype value of 176 µmol kg^{-1} in SPMW to 85 µmol kg^{-1} in the LNEADW. WTs mixing explained 94% of the variability of AOU, but the SE of 12.9 µmol kg^{-1} was larger than the measurement error of ~1 µmol kg^{-1} (Table 2).

Regarding the geographical variability within WTs, ENACW_12, the only central WT with significant presence in the four transects, showed significantly ($p < 0.01$) lower AOU levels in the Northern transect (144 µmol kg^{-1}) and higher in the Southern transect (204 µmol kg^{-1}; Table S2). In intermediate waters, AOU in SPMW and AA was also significantly higher in the Southern transect ($p < 0.05$). In deep waters, archetype AOU levels in LSW did not differ between transects, while in UNEADW, they were significantly ($p < 0.025$) higher in the Southern and Eastern transects (90–96 µmol kg^{-1}) as compared with the Northern and Western transects (83 µmol kg^{-1}).

Archetype DOC values (Figure 7b) ranged from 58.9 ± 2.5 µmol L^{-1} in SACW_18 to 43.4 ± 0.6 µmol L^{-1} in LNEADW (Table 2). The multiple regression with X_{ij} explained 63% of the DOC variability with a SE (4.0 µmol L^{-1}) that was about 3–4 times the measurement error of DOC. The addition of AOU to the multiple linear regression increased the explained variability to 70% and produced a 15% reduction of SE (Table 3). The AOU coefficient of the multiple regression, −0.026 ± 0.015 mol C mol O_2^{-1}, represents the average stoichiometric ratio of DOC to O_2 consumption for the meso- and

bathypelagic waters in the CVFZ. This ratio is independent of water mass mixing and indicates that DOC mineralisation may explain 3.6 ± 2.1% of the inorganic carbon production in the area, assuming a -O_2:C Redfield ratio of 1.4 mol O_2 mol C^{-1}. The AOU coefficient of the multiple linear regression of DOC with X_{ij} and AOU was -0.061 ± 0.032 and -0.150 ± 0.038 mol C mol O_2^{-1} for the Northern and Southern transects, respectively. Therefore, although DOC represented only 3.6 ± 2.1 % of the organic matter mineralised in the water masses of the CVFZ, it accounted for 9 ± 4 % and as much as 21 ± 5% in the Northern and Southern transects, respectively (Table S3).

DON (Figure 7c) decreased with depth from 5.1 ± 0.3 µmol L^{-1} in MMW to 3.1 ± 0.3 µmol L^{-1} in the deepest WT, LNEADW (Table 2). WTs mixing explained 44% of the variability of the distribution of DON in the CVFZ with a SE of 0.90 µmol L^{-1}, 3 times the measurement error (Table 2). R^2 increased to 46% and SE reduced by 22% when the multiple linear regression included X_{ij} and AOU as explanatory variables. When NO_3^- was included as an explanatory variable, R^2 increased to 55% and SE reduced by 19%. In this case, the NO_3^- coefficient of -0.16 ± 0.02 indicated that 16% of nitrate is produced following DON mineralisation in the CVFZ, a larger fraction than obtained for DOC and AOU (Table 3). When analysing the DON to NO_3^- coefficient of the multiple linear regression with X_{ij} and NO_3^- transect by transect, we obtained significant values only for the Northern (-0.12 ± 0.03) and Southern (-0.16 ± 0.03) transects (Table S3).

POC (Figure 7d) decreased with depth down to the MW level and then remained almost constant to the bottom. The highest concentrations of POC, 3.2 ± 1.2 and 2.7 ± 1.0 µmol L^{-1}, were found in the shallowest central waters SACW_18 and MMW, respectively (Table 2). WTs mixing explained only 26% of the POC variability in the CVFZ (Table 2), which increased to 38% when AOU was included in the multiple linear regression, accompanied by a SE reduction of 46% (Table 3). The AOU regression coefficient was -0.032 ± 0.005 mol C mol O_2^{-1} (Table 3), indicating that suspended POC mineralisation may explain 4.48 ± 0.70% of the inorganic carbon produced following organic matter mineralization in the meso- and bathypelagic waters.

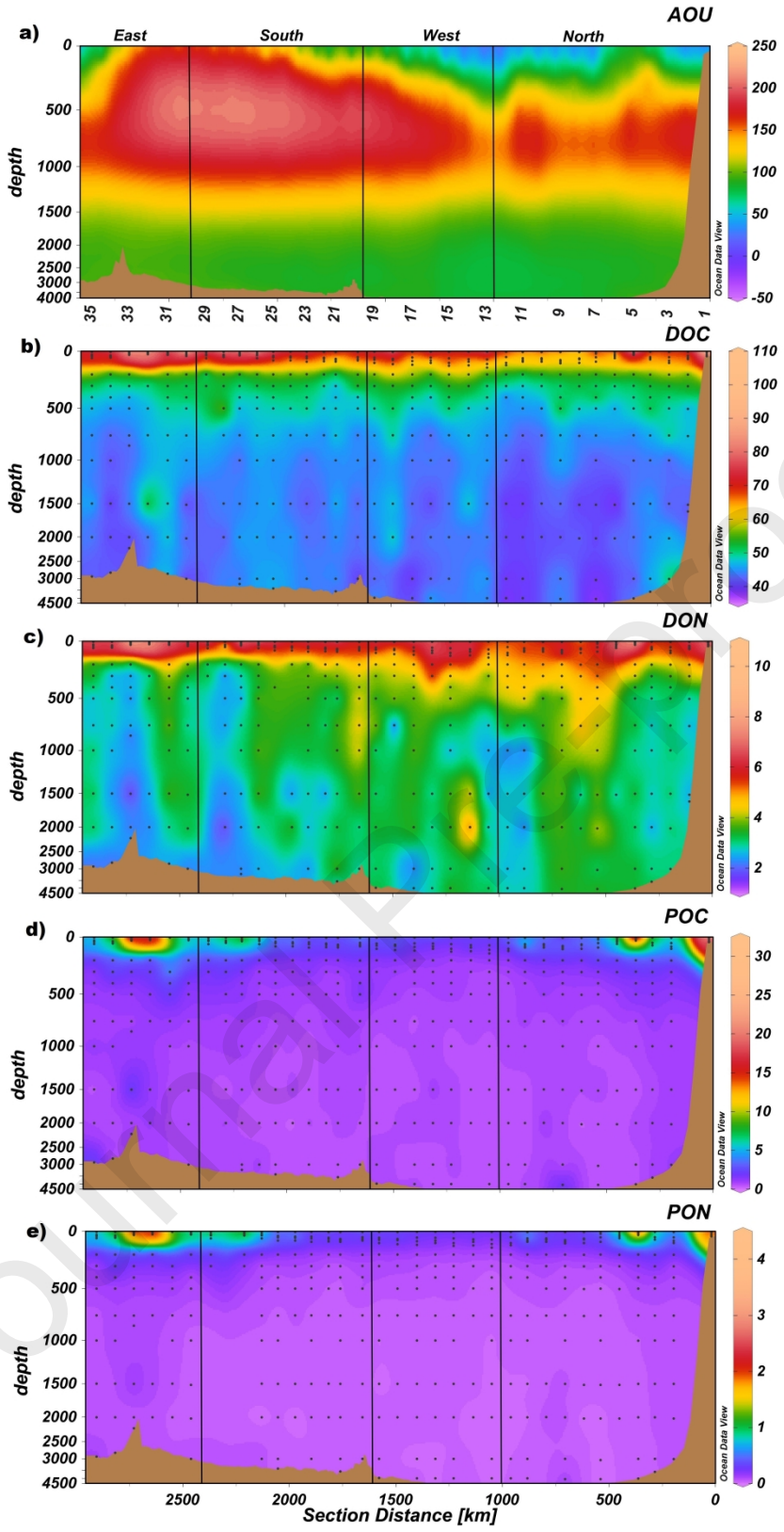

Figure 7. Full depth distributions of AOU, in µmol kg^{-1} (a), DOC in µmol L^{-1} (b), DON in µmol L^{-1} (c), POC in µmol L^{-1} (d) and PON in µmol L^{-1} (e) during the FLUXES I cruise. Dots represent samples (AOU measurements were obtaibed at 1 db vertical resolution) and vertical black lines represent the corners of the FLUXES I hydrographic box. Note that depth scale is not linear. The y-axis can be read as station number (a) or section distance in km (e). Produced with Ocean Data View (Schlitzer, 2017).

In central waters, no significant differences in POC concentration were found between transects, except for ENACW with significantly lower POC in the Western (oceanic) transect ($p < 0.025$) (Table S2, Figure 7d). In intermediate waters, POC had a subtle increase in the Eastern (coastal) transect, whereas in deep waters a slight increase was associated to LSW. Per individual transects, the variability of POC explained with the multiple regression with X_{ij} and AOU was higher than the WT mixing model though with a small SE reduction of around 5% in the Northern and Southern transects, where POC represented only 6 ± 2 % and 3 ± 1 % of the inorganic carbon produced by organic matter mineralization during water mass mixing respectively (Table S3).

Table 3. Multiple linear regressions of DOC, DON, POC and PON with the water type proportions (X_{ij}) and AOU or NO_3^-. Determination coefficient (R^2_{+1}), standard deviation (SE_{+1}), percentage of R^2 increase (%R^2) and percentage of SE reduction (%SE) between the multiple linear regression with X_{ij} (Table 2) and the multiple linear regression with X_{ij} and AOU or NO_3^-, regression coefficient of each variable with AOU or NO_3^- (β), and standard error of the estimate (SE_β) and *p*-value of β.

	DOC vs. AOU	DON vs. AOU	POC vs. AOU	PON vs. AOU	DON vs. NO_3^-	PON vs. NO_3^-
R^2_{+1}	0.70	0.46	0.38	0.44	0.50	0.34
SE_{+1}	3.4	0.7	1.0	0.10	0.73	0.13
% R^2	11	5	46	52	14	17
% SE	15	22	23	23	19	0
β	-0.0260	-0.0130	-0.0325	-0.0034	-0.1568	-0.0210
SE_β	0.0154	0.0035	0.0049	0.0005	0.0246	0.0004
p-level	0.09	0.0003	2.17E-10	4.15E-11	8.4E-10	2.99E-06

PON (Figure 7e) generally mirrored the POC distribution in central and intermediate waters. The multiple regression of PON with X_{ij} explained 29% of its variance (Table 2) and the inclusion of AOU as explanatory variable increased the explained variance to 44% with a SE reduction of 23%, while inclusion of NO_3^- increased the explained variance to 34%. The AOU coefficient was -0.0034 ± 0.001, while NO_3^- coefficient was -0.021 ± 0.004, meaning that PON covers only 2.1 ± 0.4% of NO_3^- production following organic matter mineralisation (Table 3).

The lowest PON concentrations were found in the Western (oceanic) transect, while the Northern transect presented two PON maxima in SACW_18 and MMW (Table S2). In the intermediate and deep WTs, the highest concentrations were observed in the Eastern (coastal) transect ($p < 0.01$). The variability of PON explained with the multiple

regression including X_{ij} and AOU or NO_3^- as explanatory variables was higher in the Southern than in the Northern transect (Table S3), with NO_3^- coefficients of -0.014 ± 0.002 and -0.039 ± 0.010 respectively, indicating that mineralised PON represented 1.4 ± 0.2% and 3.9 ± 1.0% of the NO_3^- produced.

Finally, the C:N molar ratio of POM increased significantly with depth from 9.9 ± 1.6 in SACW_18 to 17.3 ± 2.0 in LNEADW (Table 2). In central waters, the maximum C:N molar ratio of POM was observed in SACW_12 and ENACW_12, 12.4–12.5, while in the intermediate waters the ratio is similar for the three water masses, ranging from 14.2 to 14.5. In the deep waters, LNEADW presented the highest C:N molar ratio of POM. Concerning differences between transects, there were not significant differences in the C:N ratio of POM for ENACW_12 (Table S2). In the deep waters, the LSW presented the largest differences in C:N ratio ($p < 0.0005$) being higher in the Western transect (Table S2).

4. Discussion

4.1. Variability in the epipelagic layer of the CVFZ

The relative position of the four transects in relation to the CVF and the proximity of the Mauritanian coast explains the large differences observed in Chl-a levels and depth of the DCM between transects. The depth of the DCM ranged from 33 to 82 m, being deeper and with lower Chl-a concentration in the Western transect, as expected in oligotrophic open ocean waters (Antoine et al., 1996; Mignot et al., 2014; Iuculano et al., 2019). Conversely, the DCM was shallower and with higher Chl-a concentration in the Eastern transect, because of the impact of the offshore export of coastal plankton populations by the Cape Blanc filament (Gabric et al., 1993; Lovecchio et al., 2017; Santana-Falcón et al., 2020). The easternmost part of the Northern transect is dynamically very complex, with both cyclonic and anticyclonic eddies to the West and East of stn 5, respectively (Burgoa et al. in review). The presence of these eddies produces a convergence in stn 5 that generates the movement of the CVF to the North through this station (Figure A10, Burgoa et al. in review). This mesoscale variability at stn 5 of the Northern transect is reflected in the higher concentration of Chl-a. The front interacts with the filament of Cape Blanc, which brought organic matter across the sampling point and generated a hydrographic anomaly around this station, which presents characteristics closer to those observed to the South of the front.

NH_4^+ and NO_2^- concentrations exhibited several maxima in the surroundings of the DCM. These maxima are associated with the enhanced microbial degradation processes of ammonification and nitrification at the DCM (Ward et al., 1982; Meeder et al., 2012). It has also been suggested that the primary nitrite maximum could be related to inefficient nitrate assimilative reduction by phytoplankton at the low light levels of the DCM (Lomas and Lipschultz, 2006). The mean concentrations of NH_4^+ (0.06 µmol kg^{-1}) and NO_2^- (0.14 µmol kg^{-1}) found throughout the epipelagic layer of the CVFZ were very low, as expected for oligotrophic waters (Twomey et al., 2007; Li et al., 2008). Higher levels of 0.8 µmol kg^{-1} for NH_4^+ and 1.5 µmol kg^{-1} for NO_2^- were found in the Eastern (coastal) transect, coinciding again with the offshore export of coastal waters by the filament of Cape Blanc. These levels are comparable with those found by Clark et al. (2016) in the mixed layer of a filament in the Mauritanian upwelling.

Higher DOC concentrations in the Eastern and Southern transect, i.e. near the coast and South of the CVF, were especially noticeable at the DCM. It is expected that DOC levels are higher when approaching to the coastal ocean (Gattuso et al., 1998; del Giorgio and Duarte, 2002) and can exceed 100 µmol L^{-1} in highly productive areas such as in EBUEs (Hill and Wheeler, 2002; Hansell et al., 2009). These high DOC levels can extend offshore due to the horizontal export by the filament of Cape Blanc (Gabric et al., 1993; Lovecchio et al., 2017; 2018). The C:N ratio of DOM was also higher in the Eastern and Southern transects. The mean C:N molar ratio of DOM at the CVFZ (11.7) is slightly higher than the value of 10 mol C mol N^{-1} found by Church et al. (2002) and Hopkinson and Vallino (2005) in coastal and offshore regions of the North Atlantic and North Pacific central gyre. However, Letscher et al. (2013) found higher values around 16 mol C mol N^{-1} in the upper 50 m of Eastern Subtropical North Atlantic, (10-40ºN 10-50ºW) and South Atlantic (10-40ºS 10-50ºW).

The highest concentrations of suspended POM were also observed near the coast. Van Camp et al. (1991) and Gabric et al. (1993) estimated that the offshore currents associated with the giant filament could export around 50% of the POM produced in the coastal area around Cape Blanc (21°N). Furthermore, the differences of suspended POM concentration between the Northern and Southern transects could be explained by the passage of CVF across the Northern section around stn 5. The location of the POM

maxima in the Eastern transects coincided with the DCM, while in the Western transect POM maxima were observed at the surface.

The C:N molar ratio of POM was very variable, being the lowest near the coast i.e. along the Eastern transect (7.6 ± 0.4), because of the intense production of fresh organic matter with a lower C:N ratio in coastal waters and subsequent offshore export by the filament of Cape Blanc. Furthermore, C:N molar ratios to the North of the CVF were higher than to the South and always higher than the canonical Redfield ratio of 6.6 (Redfield et al., 1963; Anderson, 1995). In fact, Martiny et al. (2013a, b) showed large spatial variations in the C:N molar ratio of POM in the epipelagic ocean that differed substantially from the classical Redfield ratio, proposing a C:N:P ratio of 137:18:1 in warm, nutrient-rich upwelling zones. This C:N molar ratio of 7.6 is lower than the average value of 8.5, that we found down to the base of the DCM in the CVFZ.

4.2. Impact of water mass mixing in meso- and bathypelagic layers

We have applied a water mass analysis to obtain archetype DOC, DON, POC and PON concentrations for the 11 WTs identified during the FLUXES I cruise, for the entire cruise and for each transect. Our water mass analysis followed Pastor et al. (2012), except for the definition of the intermediate water AA and the deep waters. Concerning AA, its physical and chemical properties were taken in the Eastern Equatorial Atlantic, an appropriate source region because this modified Antarctic Intermediate water is transported from the equatorial region to the CVFZ by the Mauritanian current (Figure 1). Conversely, Pastor et al. (2012) took the properties of the AA in the CVFZ. Concerning the deep waters, while Pastor et al. (2012) grouped all deep WTs under the generic denomination of North Atlantic Deep Water (NADW), we identified 3 WTs: UNEADW, LNEADW and LSW, with contrasting origin and silicate concentrations (Pérez-Rodríguez et al., 2001; Álvarez and Álvarez-Salgado, 2009). With regard to the central waters, ENACW and SACW differ in their thermohaline and chemical characteristics as a result of their different origin and history from their respective formation areas to the CVFZ (Stramma and Schott, 1999). ENACW is relatively more ventilated and, therefore, well oxygenated, which explains the contrasting O_2 concentrations in relation to their position with respect to the CVF. The coexistence of the different ENACW and SACW types was evident in the large-scale distribution of water properties in the FLUXES I hydrographic box, as well as at the mesoscale range,

with the meandering of the CVF tracing the presence of low salinity central waters of southern origin in some stations of the Northern transect (Figures 3, S1).

Archetype DOC concentration in ENACW (48 to 52 μmol L^{-1}) are lower than those found in the Eastern North Atlantic by Álvarez-Salgado et al. (2013) at 40ºN and Lønborg and Álvarez Salgado (2014) at 27º–42ºN. This difference could be explained because ENACW at 40ºN is closer to the formation area and, therefore younger and DOC-richer, compared to the same water mass at 20ºN. However, in intermediate and deep waters, the DOC concentrations were similar to those found by these authors. The archetype DOC concentrations explained a major fraction (63%) of the total DOC variability in the CVFZ, suggesting that mixing and basin-scale mineralisation processes occurring from the formation area to the CVFZ are the main drivers of the DOC variability.

POC concentrations in the mesopelagic layer of the CVFZ are low, with an average value of 2.0 ± 0.5 μmol L^{-1}. Alonso-Gonzalez et al. (2009) reported higher concentrations of suspended POC in the mesopelagic layer of the Canary current from 20º to 29ºN, (3–8 μmol L^{-1}). This discrepancy is probably due the location of both sampling areas, in the core of the Canary current in Alonso-Gonzalez et al. (2009) and further South in our study. The FLUXES I box is affected by the giant filament of Cape Blanc, where higher contribution of sinking particulate material should be expected (Fischer et al., 2009). Moreover, these high sinking rates are favoured by ballasting effect of atmospheric dust inputs in the area (Bory and Newton, 2000; Fischer and Karakas, 2009). In contrast, POC concentrations in bathypelagic layers of the CVFZ are consistent with what is described by Alonso-Gonzalez et al. (2009).

The C:N ratios of suspended POM and DOM are higher than the canonical Redfield ratio and increase with depth indicating PON and DON depletion with respect to POC and DOC due to preferential remineralisation of nitrogen-rich compounds (Álvarez-Salgado et al., 2014; Hopkinson and Vallino, 2005; Letscher et al., 2013; Lønborg and Álvarez-Salgado., 2014). Previous research in the study area also found elevated, and sometimes depth dependent, C:N ratios of sinking POM, higher than the Redfield ratio (Fischer et al., 2009; 2016; Nowald et al., 2015), but always lower than the C:N ratios of suspended POM found in this work. The same trend of higher C:N ratios of suspended compared to sinking POM was observed by Schneider et al. (2003) in the subtropical gyre

of the North Pacific. We hypothesise that the larger residence time of small size suspended particles in the water column exacerbates the impact of preferential nitrogen mineralisation, explaining the higher C:N molar ratios observed.

4.3. Remineralisation of organic matter in the CVFZ

The DOC to AOU ratio obtained from the multiple linear correlation of DOC with the WT proportions and AOU suggests that DOC mineralisation explains only 3.6 ± 2.1% of the inorganic carbon production in the meso- and bathypelagic waters of the CVFZ. This surprisingly low contribution is well below the 10-20% found by Aristegui et al (2002) for the world ocean, the 26.5% to the south of the Canary Islands obtained by Aristegui et al (2003), the 9-19% obtained by Carlson et al. (2010) in the deep North Atlantic, the 28 ± 3% found by Alvarez-Salgado et al. (2013) in the subpolar North Atlantic or the 26 ± 3% by Lønborg and Alvarez-Salgado (2014) in the Eastern North Atlantic from 27º to 42ºN. The low contribution of DOC mineralisation in the CVFZ could be explained by 1) the fact that most of the water masses in this region are far away from their formation areas, where the proportion of labile DOC is higher (Hansell et al., 2012; Hansell and Carlson, 2013). In fact, we have shown that archetype DOC concentrations in the ENACW of the CVFZ are significantly lower than in areas closer to the formation area of these WTs (Alvarez-Salgado et al., 2013; Lønborg et al., 2014). And 2) the massive flux of biodegradable sinking POM produced in the coast, which is subjected to lateral export by the giant filament of Cape Blanc and sinks as the filament is moving away from the continental shelf, ballasted lithogenic materials (Iversen et al., 2010; Álvarez-Salgado and Arístegui, 2015; Lovecchio et al., 2018). As recently observed by Lopez et al. (2020) in the Eastern North Pacific, the DOC distribution in the CVFZ is apparently affected by the dissolution of these fast sinking particles, which generate columns of DOC to the bottom.

In the case of POC, it represents 4.5 ± 0.7% of the inorganic carbon production of the meso- and bathypelagic waters of the CVFZ. This contribution is far below the estimated by Alonso-González et al. (2009). They estimated that suspended POC transported laterally could account for 28% to 59% of the total mesopelagic respiration in the Canary region. The low contribution in the CVFZ suggests that the respiratory organic carbon demand in the dark ocean is mainly supported by sinking POM. In contrast, suspended POC may be exported rapidly offshore in this area of strong offshore

zonal flow, leaving a minor imprint in the biogeochemistry of the study area. This situation contrasts with the Northern location in Alonso-González et al. (2009), where the dominant mean flow is Southward and along-shore with the Canary Current, and the zonal transport is localized in mesoscale filaments and eddies (Lovecchio et al. 2017, Álvarez-Salgado et al. 2007).

The DON to NO_3^- coefficient indicates that DON supported 16% of NO_3^- produced following organic matter mineralisation. Álvarez-Salgado et al (2006) found that in NW Iberian upwelling (42ºN), the contribution of DOM to the mineralisation of organic nitrogen was 30%, while in deep open oceans waters of the North Pacific, the contribution of DON to nitrate production was from 10% to 25% (Jackson and Williams, 1985; Maita and Yanada, 1990). Mineralized PON represented only the 2.1 ± 0.4% of NO_3^-. As for the case of POC with the oxygen utilisation, the maximum contribution of mineralised PON to NO_3^- was 3.9 ± 1.1% in the Northern transect. The higher contributions of mineralised DON/PON to NO_3^- than POC/PON to oxygen utilisation support the idea that the preferential N remineralisation explains the higher Redfield POM/DOM C:N ratios in the CVFZ.

5. Conclusions

The distribution of DOM and suspended POM in the CVFZ is dictated by 1) the position of the front, which separates surface and central waters of contrasting North and South Atlantic origin, and 2) the intersection with meanders of the frontal system associated with mesoscale structures and their interaction with the giant upwelling filament of Cape Blanc. In the intermediate and deep waters, which are very distant from their respective source regions, the distributions are dictated by water mass mixing and remineralization from the source regions to the CVFZ. DOM and suspended POM mineralisation in the study hydrographic box represent only 8.1% of the carbon mineralisation and 17.8% of the nitrogen mineralisation, suggesting that 1) the local carbon demand is mainly supported by sinking POM and 2) N-containing organic compounds are mineralised faster than C-containing organic compounds.

The results obtained in this field study confirm a latitudinal gradient in the importance of the vertical vs. horizontal flows of organic matter in the Canary Current EBUE, and suggest that the offshore regions of EBUEs act as a transitional zone that

modifies the stoichiometry of the organic matter exported to the gyres, making it poor in nitrogen.

Authors' contribution

S. Valiente: Methodology, Investigation, Formal analysis, Writing - Original Draft, Visualization. **B. Fernández-Castro:** Methodology, Formal analysis, Investigation, Writing - Review & Editing, Visualization. **R. Campanero:** Investigation, Writing - Review & Editing. **A. Marrero-Díaz:** Data Curation, Investigation, Writing - Review & Editing. **A. Rodríguez-Santana:** Methodology, Investigation, Writing - Review & Editing. **M.D. Gelado-Cabellero:** Methodology, Investigation, Writing - Review & Editing. **M. Nieto-Cid:** Conceptualization, Methodology, Investigation, Writing - Review & Editing. **A. Delgado-Huertas:** Conceptualization, Writing - Review & Editing, Supervision, Funding acquisition. **J. Arístegui:** Conceptualization, Methodology, Investigation, Writing - Review & Editing, Project administration, Funding acquisition. **X.A. Álvarez-Salgado**: Conceptualization, Methodology, Formal analysis, Investigation, Writing - Original Draft, Writing - Review & Editing, Visualization, Supervision, Project administration, Funding acquisition

Acknowledgements

We would like to thank the captain and crew of R/V Sarmiento de Gamboa and the personnel of the CSIC Unidad de Tecnología Marina (UTM), for their help during the FLUXES I cruise, as well as to M.J. Pazo for DOM and POM analysis and V. Vieitez for nutrient and POM analyses. This work was supported by Spanish National Science Plan research grants FLUXES (CTM2015-69392-C3) and e-IMPACT (PID2019-109084RB-C2). S.V.R and R.C.N were supported by PhD fellowships from the Spanish Ministry of Science and Innovation (BES-2016-079216 and BES-2016-076462); B.F.C was supported by a Juan de La Cierva Formación fellowship (FJCI-641-2015-25712) and by the European Union's Horizon 2020 research and innovation program under the Marie Skłodowska-Curie grant agreement No. 834330 (SO-CUP). M.N.–C. was partially supported by the project FERMIO (MINECO, CTM2014–57334–JIN), co–financed with FEDER funds. J.A. was partly supported by the project SUMMER (AMD-817806-5) from the European Union's Horizon 2020 research and innovation program.

References

Alonso-González, I.J., Arístegui, J., Vilas, J.C., Hernández-Guerra, A., 2009. Lateral POC transport and consumption in surface and deep waters of the Canary Current region: A box model study. Global Biogeochem. Cycles 23, GB2007. https://doi.org/10.1029/2008GB003185

Alpers, W., Brandt, P., Lazar, A., Dagorne, D., Sow, B., Faye, S., Hansen, M.W., Rubino, A., Poulain, P.M., Brehmer, P., 2013. A small-scale oceanic eddy off the coast of West Africa studied by multi-sensor satellite and surface drifter data. Remote Sens. Environ. 129, 132–143. https://doi.org/10.1016/j.rse.2012.10.032

Álvarez-Salgado, X.A., Arístegui, J., Barton, E.D., Hansell, D.A., 2007. Contribution of upwelling filaments to offshore carbon export in the subtropical Northeast Atlantic Ocean. Limnol. Oceanogr. 52, 1287–1292. https://doi.org/10.4319/lo.2007.52.3.1287

Álvarez-Salgado, X.A., Nieto-Cid, M., Gago, J., Brea, S., Castro, C.G., Doval, M.D., Pérez, F.F., 2006. Stoichiometry of the degradation of dissolved and particulate biogenic organic matter in the NW Iberian upwelling. J. Geophys. Res. 111, C07017. https://doi.org/10.1029/2004JC002473

Álvarez-Salgado, X., Arístegui, J., 2015. Organic matter dynamics in the Canary Current. L. Vald. I. Déniz-González (Eds.), Oceanogr. Biol. Featur. Canar. Curr. Large Mar. Ecosyst. IOC-UNESCO, Paris (2015), pp. 151-160 (IOC Tech. Ser. No. 115).

Álvarez-Salgado, X., Nieto-Cid, M., Álvarez, M., Pérez, F., Morin, P., Mercier, H., 2013. New insights on the mineralization of dissolved organic matter in central, intermediate, and deep water masses of the northeast North Atlantic. Limnol. Oceanogr. 58, 681–696. https://doi.org/10.4319/lo.2013.58.2.0681

Álvarez, M., Álvarez-Salgado, X., 2009. Chemical tracer transport in the eastern boundary current system of the North Atlantic. Ciencias Mar. 35, 123–139. https://doi.org/10.7773/cm.v35i2.1438

Álvarez, M., Brea, S., Mercier, H., Álvarez-Salgado, X., 2014. Mineralization of biogenic materials in the water masses of the South Atlantic Ocean. I: Assessment and results of an optimum multiparameter analysis. Prog. Oceanogr. 123, 1–23. https://doi.org/10.1016/j.pocean.2013.12.007

Anderson, L.A., 1995. On the hydrogen and oxygen content of marine phytoplankton. Deep. Res. Part I 42, 1675–1680. https://doi.org/10.1016/0967-0637(95)00072-E

Antoine, D., Andre, J.M., Morel, A., 1996. Oceanic primary production: 2. Estimation

at global scale from satellite (Coastal Zone Color Scanner) chlorophyll. Global Biogeochem. Cycles 10, 57–69. https://doi.org/10.1029/95GB02832

Arístegui, J., Barton, E., Montero, M., García-Muñoz, M., Escánez, J., 2003. Organic carbon distribution and water column respiration in the NW Africa-Canaries Coastal Transition Zone. Aquat. Microb. Ecol. 33, 289–301.

Arístegui, J., Barton, E.D., Álvarez-Salgado, X.A., Santos, A., Figueiras, F.G., Kifani, S., Hernández-León, S., Mason, E., Machú, E., Demarcq, H., 2009. Sub-regional ecosystem variability in the Canary Current upwelling. Prog. Oceanogr. 83, 33–48. https://doi.org/10.1016/j.pocean.2009.07.031

Arístegui, J., Duarte, C., Agustí, S., Doval, M., Álvarez-Salgado, X., Hansell, D.A., 2002. Dissolved Organic Carbon Support of Respiration in the Dark Ocean. Sci. 2981,967.

Arístegui, J., Montero, M., Hernández-Hernández, N., Alonso-González, I., Baltar, F., Calleja, M.L., Duarte, C.M., 2020. Variability in Water-Column Respiration and Its Dependence on Organic Carbon Sources in the Canary Current Upwelling Region. Front. Earth Sci. 8, 349. https://doi.org/10.3389/feart.2020.00349

Barceló-Llull, B., Sangrà, P., Pallàs-Sanz, E., Barton, E.D., Estrada-allis, S.N., Martínez-Marrero, A., Aguiar-Gonzalez, B., Grisolla, D., Gordo, C., Rodríguez-Santana, Á., Marrero-Díaz, Á., Arístegui, J., 2017. Anatomy of a subtropical intrathermocline eddy. Deep. Res. Part I Oceanogr. Res. Pap. 124, 126–139.

Barton, E., Arıstegui, J., Tett, P., Cantón, M., García- Braun, J., Hernández-León, S., Nykjaer, L., Almeida, C., Almunia, J., Ballesteros, S., Basterretxea, G., Escánez, J., García-Weil, L., Hernandez-Guerra, A., López-Laatzen, F., Molina, R., Montero, M., Navarro-Pérez, E., Rodríguez, J., Van Lenning, K., Wild, K., 1998. The transition zone of the Canary Current upwelling region. Prog. Oceanogr. 41, 455–504.

Bory, A.J.-M., Newton, P.P., 2000. Transport of airborne lithogenic material down through the water column in two contrasting regions of the eastern subtropical North Atlantic Ocean. Global Biogeochem. Cycles 14, 297–315. https://doi.org/10.1029/1999gb900098

Boyd, P., Claustre, H., Levy, M., Siegel, D., Weber, T., 2019. Multi-faceted particle pumps drive carbon sequestration in the ocean. Nature 568, 327–336.

Broecker, W.S., 1974. NO a conservative water–mass tracer. Earth Planet. Sci. Lett. 23 100–107.

Burgoa, N., Machín, F., Marrero-Díaz, S., Rodríguez-Santana, A., Martínez-Marrero, A., Arístegui, J., Duarte, C., 2020. Mass, nutrients and dissolved organic carbon (DOC) lateral transports off northwest Africa during fall 2002 and spring 2003 Item Type Article. Ocean Sci. 16, 483–511. https://doi.org/10.5194/os-16-483-2020

Cardoso, C., Caldeira, R.M.A., Relvas, P., Stegner, A., 2020. Islands as eddy transformation and generation hotspots: Cabo Verde case study. Prog. Oceanogr. 184, 102271. https://doi.org/10.1016/j.pocean.2020.102271

Carlson, C., Hansell, D., Nelson, N., Siegel, D., 2010. Dissolved organic carbon export and subsequent remineralization in the mesopelagic and bathypelagic realms of the North Atlantic basin. Deep Sea Res. Part II 57, 1433–1445.

Church, M.J., Ducklow, H.W., Karl, D.M., 2002. Multiyear increases in dissolved organic matter inventories at Station ALOHA in the North Pacific Subtropical Gyre. Limnol. Oceanogr. 47, 1–10. https://doi.org/10.4319/lo.2002.47.1.0001

Clark, D.R., Widdicombe, C.E., Rees, A.P., Woodward, E., 2016. The significance of nitrogen regeneration for new production within a filament of the Mauritanian upwelling system. Biogeosciences 13, 2873–2888. https://doi.org/10.5194/bg-13-2873-2016

Del Giorgio, P., Duarte, C., 2002. Respiration in the open ocean. Nature 420, 379–384.

Fischer, G., Karakaş, G., 2009. Sinking rates and ballast composition of particles in the Atlantic Ocean: implications for the organic carbon fluxes to the deep ocean. Biogeosciences 6, 85–102. https://doi.org/10.5194/bg-6-85-2009

Fischer, G., Reuter, C., Karakas, G., Nowald, N., Wefer, G., 2009. Offshore advection of particles within the Cape Blanc filament, Mauritania: Results from observational and modelling studies. Prog. Oceanogr. 83, 322–330.

Fischer, G., Romero, O., Toby, E., Iversen, M., Donner, B., Mollenhauer, G., Nowald, N., Ruhland, G., Klann, M., Hamady, B., Wefer, G., 2019. Changes in the Dust-Influenced Biological Carbon Pump in the Canary Current System: Implications From a Coastal and an Offshore Sediment Trap Record Off Cape Blanc, Mauritania. Global Biogeochem. Cycles 33, 1100–1128. https://doi.org/10.1029/2019GB006194

Gabric, A.J., Garcia, L., Van Camp, L., Nykjaer, L., Eifler, W., Schrimpf, W., 1993. Offshore export of shelf production in the Cape Blanc (Mauritania) giant filament as derived from coastal zone color scanner imagery. J. Geophys. Res. 98, 4697–

4712. https://doi.org/10.1029/92JC01714

Gattuso, J.-P., Frankignoulle, M., Wollast, R., 1998. Carbon and Carbonate metabolism in coastal aquatic ecosystems. Annu. Rev. Ecol. Syst. 29, 405–434. https://doi.org/10.1146/annurev.ecolsys.29.1.405

Hansell, D.A., Carlson, C.A., 2013. Localized refractory dissolved organic carbon sinks in the deep ocean. Global Biogeochem. Cycles 27, 705–710. https://doi.org/10.1002/gbc.20067

Hansell, D.A., Carlson, C.A., Schlitzer, R., 2012. Net removal of major marine dissolved organic carbon fractions in the subsurface ocean. Global Biogeochem. Cycles 26, GB1016. https://doi.org/10.1029/2011GB004069

Hansell, D., Carlson, C., Repeta, D., Schlitzer, R., 2009. Dissolved organic matter in the ocean: A controversy stimulates new insights. Oceanography 22, 202–211.

Hansen, H., Koroleff, F., 1999. Methods of Seawater Analysis, 3rd, Completely Revised and Extended Edition, Ed. by K. Grashoff et al (Wiley, Weinheim, 1999), pp. 149–228.

Helmke, P., Romero, O., Fischer, G., 2005. Northwest African upwelling and its effect on offshore organic carbon export to the deep sea. Global Biogeochem. Cycles 19, GB4015. https://doi.org/10.1029/2004GB002265

Hill, J.K., Wheeler, P.A., 2002. Organic carbon and nitrogen in the northern California current system: comparison of offshore, river plume, and coastally upwelled waters. Prog. Oceanogr. 53, 369–387.

Holm-Hansen, O., Lorenzen, C.J., Holmes, R.W., Strickland, J.D.H., 1965. Fluorometric Determination of Chlorophyll. ICES J. Mar. Sci. 30, 3–15. https://doi.org/10.1093/icesjms/30.1.3

Hopkinson, C., Vallino, J., 2005. Efficient export of carbon to the deep ocean through dissolved organic matter. Nature 433, 142–145.

Iuculano, F., Álvarez-Salgado, X., Otero, J., Catalá, T., Sobrino, C., Duarte, C., Agustí, S., 2019. Patterns and drivers of UV absorbing chromophoric dissolved organic matter in the euphotic layer of the open ocean. Front. Mar. Sci. 6, 320.

Iversen, M., Nowald, N., Ploug, H., Jackson, G., Fischer, G., 2010. High resolution profiles of vertical particulate organic matter export off Cape Blanc, Mauritania: Degradation processes and ballasting effects. Deep. Res. Part I 57, 771–784.

Jackson, G.A., Williams, P.M., 1985. Importance of dissolved organic nitrogen and phosphorus to biological nutrient cycling. Deep Sea Res. Part A, Oceanogr. Res.

Pap. 32, 223–235. https://doi.org/10.1016/0198-0149(85)90030-5

Karakaş, G., Nowald, N., Blaas, M., Marchesiello, P., Frickenhaus, S., Schlitzer, R., 2006. High-resolution modeling of sediment erosion and particle transport across the northwest African shelf. J. Geophys. Res. 111, C06025. https://doi.org/10.1029/2005JC003296

Karstensen, J., Tomczak, M., 1998. Age determination of mixed water masses using CFC and oxygen data. J. Geophys. Res. 103, 18599–18609. https://doi.org/10.1029/98JC00889

Kérouel, R., Aminot, A., 1997. Fluorometric determination of ammonia in sea and estuarine waters by direct segmented flow analysis. Mar. Chem. 57, 265–275. https://doi.org/10.1016/S0304-4203(97)00040-6

Langdon, C., 2010. Determination of dissolved oxygen in seawater by winkler titration using the amperometric technique. Hood, E.M., Sloyan, B.M., Sabine, C. (Eds.), Go-sh. Repeat Hydrogr. Man. A Collect. Expert Reports Guidel. IOCCP Rep. no. 14, ICPO Publ. Ser. no. 134.

Letscher, R.T., Hansell, D.A., Carlson, C.A., Lumpkin, R., Knapp, A.N., 2013. Dissolved organic nitrogen in the global surface ocean: Distribution and fate. Global Biogeochem. Cycles 27, 141–153. https://doi.org/10.1029/2012GB004449

Li, Q.P., Hansell, D.A., Zhang, J.-Z., 2008. Underway monitoring of nanomolar nitrate plus nitrite and phosphate in oligotrophic seawater. Limnol. Oceanogr. Methods 6, 319–326. https://doi.org/10.4319/lom.2008.6.319

Lomas, M.W., Lipschultz, F., 2006. Forming the primary nitrite maximum: Nitrifiers or phytoplankton? Limnol. Oceanogr. https://doi.org/10.4319/lo.2006.51.5.2453

Lønborg, C. and, Álvarez-Salgado, 2014. Tracing dissolved organic matter cycling in the eastern boundary of the temperate North Atlantic using absorption and fluorescence spectroscopy. Deep. Res. I 85, 35–46.

Lopez, C.N., Robert, M., Galbraith, M., Bercovici, S.K., Orellana, M. V., Hansell, D.A., 2020. High Temporal Variability of Total Organic Carbon in the Deep Northeastern Pacific. Front. Earth Sci. 8, 80. https://doi.org/10.3389/feart.2020.00080

Lovecchio, E., Gruber, N., Münnich, M., 2018. Mesoscale contribution to the long-range offshore transport of organic carbon from the Canary Upwelling System to the open North Atlantic. Biogeosciences 15, 2018–5061. https://doi.org/10.3929/ethz-b-000286944

Lovecchio, E., Gruber, N., Münnich, M., Lachkar, Z., 2017. On the long-range offshore transport of organic carbon from the Canary Upwelling System to the open North Atlantic. Biogeosciences 14, 3337–3369. https://doi.org/10.3929/ethz-b-000190480

Maita, Y., Yanada, M., 1990. Vertical distribution of total dissolved nitrogen and dissolved organic nitrogen in seawater. Geochem. J. 24, 245–254. https://doi.org/10.2343/geochemj.24.245

Martínez-Marrero, A., Rodríguez-Santana, A., Hernández-Guerra, A., Fraile-Nuez, E., López-Laatzen, F., Vélez-Belchí, P., Parrilla, G., 2008. Distribution of water masses and diapycnal mixing in the Cape Verde Frontal Zone. Geophys. Res. Lett. 35, L07609. https://doi.org/10.1029/2008GL033229

Martiny, A., Vrugt, J., Primeau, F., Lomas, M., 2013. Regional variation in the particulate organic carbon to nitrogen ratio in the surface ocean. Global Biogeochem. Cycles 27, 723–731. https://doi.org/10.1002/gbc.20061

Martiny, A.C., Pham, C.T.A., Primeau, F.W., Vrugt, J.A., Moore, J.K., Levin, S.A., Lomas, M.W., 2013. Strong latitudinal patterns in the elemental ratios of marine plankton and organic matter. Nat. Geosci. 6, 279–283. https://doi.org/10.1038/ngeo1757

Meeder, E., Mackey, K., Paytan, A., Shaked, Y., Iluz, D., Stambler, N., Rivlin, T., Post, A., Lazar, B., 2012. Nitrite dynamics in the open ocean—clues from seasonal and diurnal variations. Mar. Ecol. Prog. Ser. 453, 11–26. https://doi.org/10.3354/meps09525

Meunier, T., Barton, E., Barreiro, B., Torres, R., 2012. Upwelling filaments off cap blanc: Interaction of the NW african upwelling current and the cape verde frontal zone eddy field? J. Geophys. Res. 117, C08031. https://doi.org/10.1029/2012JC007905

Mignot, A., Claustre, H., Uitz, J., Poteau, A., D'Ortenzio, F., Xing, X., 2014. Understanding the seasonal dynamics of phytoplankton biomass and the deep chlorophyll maximum in oligotrophic environments: A Bio-Argo float investigation. Global Biogeochem. Cycles 28, 856– 876. https://doi.org/10.1002/2013GB004781

Nowald, N., Iversen, M., Fischer, G., Ratmeyer, V., Wefer, G., 2015. Time series of in-situ particle properties and sediment trap fluxes in the coastal upwelling filament off Cape Blanc, Mauritania. Prog. Oceanogr. 137, 1–11.

https://doi.org/10.1016/j.pocean.2014.12.015

Nowald, N., Karakas, G., Ratmeyer, V., Fischer, G., Schlitzer, R., Davenport, R.A., Wefer, G., 2006. Distribution and transport processes of marine particulate matter off Cape Blanc (NW-Africa): results from vertical camera profiles. Ocean Sci. Discuss 3, 903–938.

Ohde, T., Fiedler, B., Körtzinger, A., 2015. Spatio-temporal distribution and transport of particulate matter in the eastern tropical North Atlantic observed by Argo floats. Deep. Res. Part I 102, 26–42.

Olivar, M., Sabatés, A., Pastor, M., Pelegrí, J., 2016. Water masses and mesoscale control on latitudinal and cross-shelf variations in larval fish assemblages off NW Africa. Deep. Res. Part I Oceanogr. Res. Pap. 117, 120–137. https://doi.org/10.1016/j.dsr.2016.10.003

Pastor, M., Peña-Izquierdo, J., Pelegrí, J., Marrero-Díaz, A., 2012. Meridional changes in water mass distributions off NW Africa during November 2007/2008. Ciencias Mar. 38, 223– 244. https://doi.org/10.7773/cm.v38i1B.1831

Pelegrí, J.L., Peña-Izquierdo, J., 2015. Easter boundary currents off North'West Africa. Oceanogr. Biol. Featur. Canar. Curr. Large Mar. Ecosyst. 3 81-92 , IOC Tech. Ser. 115 81–92 IOC Technical Series.

Pérez-Rodríguez, P., Pelegrí, J., Marrero-Díaz, A., 2001. Dynamical characteristics of the Cape Verde frontal zone. Mar. Sci. 65, 241–250.

Redfield, A.C., Ketchum, B., Richards, F., 1963. The influence of organisms on the composition of seawater. "'The Sea'" (Hill, M. N., ed.). Vol. 2, Wiley-Interscience, New York. pp. 26–77.Richards, F. A.

Repeta, D.J., 2015. Chemical Characterization and Cycling of Dissolved Organic Matter, in: Biogeochemistry of Marine Dissolved Organic Matter: Second Edition. Elsevier Inc., pp. 21–63. https://doi.org/10.1016/B978-0-12-405940-5.00002-9

Sangrà, P., Pascual, A., Rodríguez-Santana, Á., Machín, F., Mason, E., McWilliams, J.C., Pelegrí, J.L., Dong, C., Rubio, A., Arístegui, J., Marrero-Díaz, Á., Hernández-Guerra, A., Martínez-Marrero, A., Auladell, M., 2009. The Canary Eddy Corridor: A major pathway for long-lived eddies in the subtropical North Atlantic. Deep. Res. Part I Oceanogr. Res. Pap. 56, 2100–2114. https://doi.org/10.1016/j.dsr.2009.08.008

Santana-Falcón, Y., Mason, E., Arístegui, J., 2020. Offshore transport of organic carbon by upwelling filaments in the Canary Current System. Prog. Oceanogr. 186,

102322. https://doi.org/10.1016/j.pocean.2020.102322

Schlitzer, R., 2017. Ocean Data View. Ocean Data View.

Schneider, B., Schlitzer, R., Fischer, G., Nöthig, E.M., 2003. Depth-dependent elemental compositions of particulate organic matter (POM) in the ocean. Global Biogeochem. Cycles 17. https://doi.org/10.1029/2002gb001871

Stramma, L., Schott, F., 1999. The mean flow field of the tropical Atlantic Ocean. Deep. Res. II 46, 279–303.

Tiedemann, M., Fock, H., Döring, J., Bonaventure-Badji, L., Möllmann, C., 2018. Water masses and oceanic eddy regulation of larval fish assemblages along the Cape Verde Frontal Zone. J. Mar. Syst. 183, 42–55.

Tomczak, M., 1999. Some historical, theoretical and applied aspects of quantitative water mass analysis. J. Mar. Res. 57, 275–303. https://doi.org/10.1357/002224099321618227

Twomey, L.J., Waite, A.M., Pez, V., Pattiaratchi, C.B., 2007. Variability in nitrogen uptake and fixation in the oligotrophic waters off the south west coast of Australia. Deep. Res. Part II Top. Stud. Oceanogr. 54, 925–942. https://doi.org/10.1016/j.dsr2.2006.10.001

UNESCO, 1986. Progresson Oceanographic Tables and Standards 1983–1986.Work and Recommendations of the UNESCO/SCOR/ICES/IAPSO Joint Panel.UNESCO Technical Papers in Marine Science 50.

Van Camp, L., Nykjaer, L., Mittelstaedt, E., Schlittenhardy, P., 1991. Upwelling and boundary circulation off Northwest Africa as depicted by infrared and visible satellite observations. Prog. Oceanogr. 26, 357–402.

Verdugo, P., Alldredge, A.L., Azam, F., Kirchman, D.L., Passow, U., Santschi, P.H., 2004. The oceanic gel phase: a bridge in the DOM-POM continuum. Mar. Chem. 92, 67–85. https://doi.org/10.1016/j.marchem.2004.06.017

Ward, B.B., Olson, R.J., Perry, M.J., 1982. Microbial nitrification rates in the primary nitrite maximum off southern California. Deep Sea Res. Part A, Oceanogr. Res. Pap. 29, 247–255. https://doi.org/10.1016/0198-0149(82)90112-1

Zenk, W., Klein, B., Schroder, M., 1991. Cape Verde Frontal Zone. Deep Sea Res. Part A 38, S505–S530. https://doi.org/10.1016/S0198-0149(12)80022-7

Declaration of interests

☒ The authors declare that they have no known competing financial interests or personal relationships that could have appeared to influence the work reported in this paper.

☐ The authors declare the following financial interests/personal relationships which may be considered as potential competing interests: